

$\alpha_s v^2$ corrections to η_c and χ_{cJ} production recoiled with a photon at e^+e^- colliders

Guang-Zhi Xu ^a, Yi-Jie Li ^b, Kui-Yong Liu ^b, Yu-Jie Zhang^{a,c}

^a*School of Physics, Beihang University, Beijing 100191, China*

^b*Department of Physics, Liaoning University, Shenyang 110036, China*

^c*CAS Center for Excellence in Particle Physics, Beijing 100049, China*

E-mail: still200@gmail.com, yijiegood@gmail.com,
liukuiyong@lnu.edu.cn, nophy0@gmail.com

ABSTRACT: We consider the production of the η_c and χ_{cJ} states recoiled with a photon up to $\mathcal{O}(\alpha_s v^2)$ at BESIII and B-factories within the frame of NRQCD factorization. With the corrections, we revisit the numerical calculations to the cross sections for the $\eta_c(nS)$ and the $\chi_{cJ}(mP)$ states. We argue that the search for XYZ states with even charge conjugation such as $X(3872)$, $X(3940)$, $X(4160)$, and $X(4350)$ recoiled with a photon at BESIII may help clarify the nature of these states. For completeness, the production of charmonium with even charge conjugation recoiled with a photon at B factories is also discussed.

Contents

1	Introduction	1
2	The framework of the calculation	2
2.1	Kinematics	3
2.2	Amplitudes expansion	5
2.3	One-loop computation	7
2.4	Matching results for η_c	8
2.5	Matching results for χ_{cJ}	10
3	Cross section	11
3.1	η_c	12
3.2	χ_{cJ}	12
4	Numerical results and discussion	14
5	Summary	19
6	Appendix	20

1 Introduction

Non-relativistic quantum chromodynamics (NRQCD) is a rigorous and successful effect field theory that describes heavy quarkonium decay and production[1]. The color-octet mechanics (COM) is proposed in NRQCD. The infrared divergences in the decay widths of P -wave [2, 3] and D -wave [4–6] heavy quarkonium have been absorbed into the NRQCD matrix elements applied with COM, and the infrared-safe decay rate can be obtained. But the last decade experiment measurements at e^+e^- colliders and at hadron colliders reveal large discrepancies with LO (leading order) calculations.

In the e^+e^- annihilation experiment[7, 8], problems on NRQCD involving the inclusive and exclusive J/ψ production[9–14] had been solved by higher-order corrections, including radiative corrections[15–26], relativistic corrections[27–35], and $\mathcal{O}(\alpha_s v^2)$ corrections [36, 37]. And the LO NRQCD calculations at hadron colliders also encounters dilemma in the heavy quarkonium production and polarization especially at the large p_t region. The contributions from the NLO (next-to-leading order) radiative corrections to the heavy quarkonium production [38–53] and polarization [54–59] at hadron colliders are significant. And the contributions of the NLO relativistic corrections to J/ψ hadronic production are considered too[60–62].

$\mathcal{O}(\alpha_s v^2)$ corrections to the decays of h_c, h_b and η_b are studied in Ref.[63–65]. Actually, the corrections at higher-order(e.g., $\mathcal{O}(\alpha_s v^2), v^4$), had been considered in many processes and contributed considerable effects. However, some drawbacks for fixed-order calculations involve the convergence for higher-order corrections and to which order should be considered within NRQCD. These problems can be understood by adding more higher-order calculations. More information about NRQCD can be found in Ref.[66] and related papers.

Studies have focused on the production of quarkonium with even charge conjugation that are recoiled with a hard photon in the e^+e^- annihilation at the B factories and BESIII is a very interesting process. The production of double charmonium at B factories[7, 8] aids in identifying to identify charmonium or charmonium-like states with even charge conjugation, which recoiling with J/ψ and $\psi(2S)$. $\eta_c, \eta_c(2S), \chi_{c0}, X(3940)$ (decaying into $D\bar{D}^*$), and $X(4160)$ (decaying into $D^*\bar{D}^*$) have also been observed in double charmonium production at B factories, but the χ_{c1} and χ_{c2} states are yet to be determined in production associated with J/ψ at B factories. The LO calculation for heavy quarkonium with even charge conjugation recoiled with a hard photon in the e^+e^- annihilation at the B factories and BESIII is a pure QED process[67, 68]. The one-loop calculations have been computed and analyzed[69–73]. And the NLO relativistic corrections have been computed too [70, 72]. Quarkonium with even charge conjugation are associated to the XYZ particles[74–76]. The well-known one of the XYZ particles, $X(3872)$ [77], is supposed to the χ'_{c1} state or the mixture of this state with other structure in some view[49, 78]. Recently, $X(3872)$ has been observed in photon-recoiled process with a statistical significance of 6.4σ at BESIII[79]. $X(3915)$ ($X(3945)$ or $Y(3940)$) and $Z(3930)$ are assigned as the $\chi_{c0}(2P)$ and $\chi_{c2}(2P)$ states by the PDG (Particle Data Group)[80]. However this identification may be called into some questions[81]. The experimental results for states with even charge conjugation have theoretically elicited interest in the nature of charmonium-like states. The non-perturbative effects are strong because the energy region at BESIII approximates the threshold charmonium states. Hence, the applicability of NRQCD is speculative within this region. However, some NRQCD-based calculations exhibit high compatibility with the data.

In this paper, the photon-recoiled η_c and χ_{cJ} production is studied according to our previous work[72]. We calculate the cross sections up to the order of $\mathcal{O}(\alpha_s v^2)$ within the NRQCD. This study verifies the applicability of NRQCD at the threshold and determines the XYZ particles related to $\eta_c(nS)$ and $\chi_{cJ}(nP)$.

The paper is organized as follows. Sec.2 introduces the framework of calculations, especially the method of the expansion up to $(\alpha_s v^2)$ for the amplitudes. Sec.3 presents the amplitudes expansion and discussion the cross sections for the η_c and χ_{cJ} process. Sec.4 gives the numerical results up to $\mathcal{O}(\alpha_s v^2)$. Finally, Sec.5 presents a summary.

2 The framework of the calculation

This section introduces the calculation method for the $\mathcal{O}(\alpha_s v^2)$ amplitude expansion to the process $e^+e^- \rightarrow \gamma^* \rightarrow H(\eta_c, \chi_{cJ}) + \gamma$. The momenta of final states are stated as $H(p)$ and

$\gamma(k)$. Cross section can be obtained and applied to express the amplitudes via expansions.

2.1 Kinematics

In an arbitrary frame of the charmonium, the momenta of the charm and the anti-charm can be expressed by the meson momentum and their relative momentum,

$$\begin{aligned} p_c &= p/2 + q, \\ p_{\bar{c}} &= p/2 - q. \end{aligned} \quad (2.1)$$

The momenta p and q are orthogonal, i.e., $p \cdot q = 0$. In the meson rest frame, they can be written as, $p = (2E_q, \mathbf{0})$ and $q = (0, \mathbf{q})$. We calculated the amplitudes up to the order $\mathcal{O}(\alpha_s v^2)$ using an orthodox method. In this method, the rest energy $E_q = \sqrt{m_c^2 + \mathbf{q}^2}$ of the charm/anti-charm should be expanded around the charm mass,

$$E_q = m_c + \frac{\mathbf{q}^2}{m_c^2} \frac{m_c}{2} + \mathcal{O}\left(\frac{\mathbf{q}^4}{m_c^4}\right). \quad (2.2)$$

The momenta of the final-state particles depend on E_q . For instance, the four-momenta of the particles in $\gamma^*(Q) \rightarrow H(p) + \gamma(k)$ in the center-of-mass system can be written as follows:

$$\begin{aligned} Q &= (\sqrt{s}, 0, 0, 0), \\ p &= \left(\frac{s + 4E_q^2}{2\sqrt{s}}, 0, 0, \frac{s - 4E_q^2}{2\sqrt{s}}\right), \\ k &= \left(\frac{s - 4E_q^2}{2\sqrt{s}}, 0, 0, -\frac{s - 4E_q^2}{2\sqrt{s}}\right). \end{aligned} \quad (2.3)$$

Given the expression for E_q , the four-momenta can be expanded in terms of \mathbf{q}^2/m_c^2 . For instance, the momenta of the final meson and the photon noted by p and k are expanded as the following expression,

$$\begin{aligned} p &= \left(\frac{s + 4m_c^2}{2\sqrt{s}}, 0, 0, \frac{s - 4m_c^2}{2\sqrt{s}}\right) + \frac{\mathbf{q}^2}{m_c^2} \frac{2m_c^2}{\sqrt{s}} (1, 0, 0, -1) + \mathcal{O}\left(\frac{\mathbf{q}^4}{m_c^4}\right) \\ &= p^{(0)} + \frac{\mathbf{q}^2}{m_c^2} p^{(2)} + \mathcal{O}\left(\frac{\mathbf{q}^4}{m_c^4}\right), \\ k &= \frac{s - 4m_c^2}{2\sqrt{s}} (1, 0, 0, -1) - \frac{\mathbf{q}^2}{m_c^2} \frac{2m_c^2}{\sqrt{s}} (1, 0, 0, -1) + \mathcal{O}\left(\frac{\mathbf{q}^4}{m_c^4}\right) \\ &= k^{(0)} + \frac{\mathbf{q}^2}{m_c^2} k^{(2)} + \mathcal{O}\left(\frac{\mathbf{q}^4}{m_c^4}\right). \end{aligned} \quad (2.4)$$

Therefore, the momenta with subscripts (0) or (2) are independent of \mathbf{q}^2 . The scalar products of $(p^{(0)}, p^{(2)}, k^{(0)}, \text{ and } k^{(2)})$ can be solved in a special frame. For instance, in the center-of-mass system, the relation $k^{(2)} = -p^{(2)}$ can be obtained to reduce the number of the independent

momenta; all the three non-zero products are calculated as follows:

$$\begin{aligned} p^{(0)} \cdot p^{(0)} &= 4m_c^2, \\ p^{(0)} \cdot p^{(2)} &= 2m_c^2, \\ p^{(0)} \cdot k^{(0)} &= (s - 4m_c^2)/2. \end{aligned} \quad (2.5)$$

Studies on the $\mathcal{O}(\alpha_s v^2)$ corrections to the decay process of charmonium with massless final-states([63–65, 82]) introduce a factor E_q/m_c to all external momenta. In our method, these momenta can be expanded as $p_i = p_i^{(0)} + \frac{\mathbf{q}^2}{m_c^2} p_i^{(2)} = p_i^{(0)}(1 + \frac{\mathbf{q}^2}{2m_c^2})$ with $p_i^{(2)} = p_i^{(0)}/2$. This equation indicates the compatibility of our method with that published.

For the P -wave states, the spin and orbital vectors must also be expanded by

$$\begin{aligned} \epsilon_s &= \epsilon_s^{(0)} + \frac{\mathbf{q}^2}{m_c^2} \epsilon_s^{(2)} + \mathcal{O}(\frac{\mathbf{q}^4}{m_c^4}), \\ \epsilon_L &= \epsilon_L^{(0)} + \frac{\mathbf{q}^2}{m_c^2} \epsilon_L^{(2)} + \mathcal{O}(\frac{\mathbf{q}^4}{m_c^4}), \end{aligned} \quad (2.6)$$

Furthermore, they couple onto the total angular momentum J states ($J = 0, 1, 2$) with the relation presented as follows:

$$\begin{aligned} \mathcal{P}_0^{\alpha\beta} &\equiv \sum_{s_z L_z} \epsilon_s^{*\alpha} \epsilon_L^{*\beta} \langle 1s_z; 1L_z | 00 \rangle = \frac{1}{\sqrt{D-1}} \Pi^{\alpha\beta}, \\ \mathcal{P}_1^{\alpha\beta} &\equiv \sum_{s_z L_z} \epsilon_s^{*\alpha} \epsilon_L^{*\beta} \langle 1s_z; 1L_z | 1J_z \rangle = \frac{i}{\sqrt{2}M} \epsilon^{\alpha\beta\kappa\lambda} p_\kappa \epsilon_\lambda^*(J_z), \\ \mathcal{P}_2^{\alpha\beta} &\equiv \sum_{s_z L_z} \epsilon_s^{*\alpha} \epsilon_L^{*\beta} \langle 1s_z; 1L_z | 2J_z \rangle = \epsilon^{*\alpha\beta}(J_z). \end{aligned} \quad (2.7)$$

The polarization is summed over all directions of the vector for the total angular momentum:

$$\begin{aligned} \sum_{J_z} \epsilon^\alpha(J_z) \epsilon^{*\beta}(J_z) &= \Pi^{\alpha\beta}, \\ \sum_{J_z} \epsilon^{\alpha\beta} \epsilon^{*\alpha'\beta'} &= \frac{1}{2} (\Pi^{\alpha\alpha'} \Pi^{\beta\beta'} + \Pi^{\alpha\beta'} \Pi^{\alpha'\beta}) - \frac{1}{D-1} \Pi^{\alpha\beta} \Pi^{\alpha'\beta'}, \end{aligned} \quad (2.8)$$

where Π can be expanded in terms of \mathbf{q} :

$$\begin{aligned} \Pi_{\alpha\beta} &\equiv -g_{\alpha\beta} + \frac{p_\alpha p_\beta}{p^2}, \\ \Pi_{\alpha\beta} &= \Pi_{\alpha\beta}^{(0)} + \frac{\mathbf{q}^2}{4m_c^2} (p_\alpha^{(0)} p_\beta^{(2)} + p_\alpha^{(2)} p_\beta^{(0)} - p_\alpha^{(0)} p_\beta^{(0)}) + \mathcal{O}(\frac{\mathbf{q}^4}{m_c^4}). \end{aligned} \quad (2.9)$$

The second term vanishes in the rest frame of the meson, which is consistent with the independence of the polarization vectors to \mathbf{q}^2 in this frame.

2.2 Amplitudes expansion

The amplitude of $e^+e^- \rightarrow \gamma H(\eta_c, \chi_{cJ})$ can be written as[30]

$$\mathcal{M}(e^+e^- \rightarrow \gamma H) = L_\alpha \mathcal{M}^\alpha(\gamma^* \rightarrow \gamma H), \quad (2.10)$$

where the leptonic part L_α is independent of \mathbf{q} . We only consider the hadronic part element $\mathcal{M}^\alpha(\gamma^* \rightarrow \gamma H)$ in the NRQCD frame. The Feynman diagrams are shown in Fig.1. The amplitude can be written as[30]:

$$\mathcal{M}(\gamma^* \rightarrow \gamma H) = \sqrt{2M_H} \sum_n d_n \langle H | \mathcal{O}_n^H | 0 \rangle, \quad (2.11)$$

where the factor $\sqrt{2M_H}$ originates from the relativistic normalization. d_n is the short-distance coefficient that can be obtained by matching with the full QCD calculations on the intermediate $c\bar{c}$ production. And the $\langle H | \mathcal{O}_n^H | 0 \rangle$ represents the NRQCD long-distance matrix elements that are extracted from the experimental data or determined by potential model or lattice calculations. The present study concentrates on the corrections up to the order $\mathcal{O}(\alpha_s v^2)$ under the color-singlet frame. The expansion is given as follows:

$$\begin{aligned} \mathcal{M}(\gamma^* \rightarrow \gamma H) &= \sqrt{2M_H} [(d^{(0)} + d^{(\alpha_s)}) \langle H | \mathcal{O}^H | 0 \rangle + (d^{(v^2)} + d^{(\alpha_s v^2)}) \langle H | \mathcal{P}^H | 0 \rangle] \\ &\approx 2\sqrt{m_c} (1 + \frac{\mathbf{q}^2}{4m_c^2}) [(d^{(0)} + d^{(\alpha_s)}) \langle H | \mathcal{O}^H | 0 \rangle + (d^{(v^2)} + d^{(\alpha_s v^2)}) \langle H | \mathcal{P}^H | 0 \rangle]. \end{aligned} \quad (2.12)$$

The short-distance coefficients are obtained from the matching between the pQCD and the NRQCD calculations on the $c\bar{c}$ production,

$$\begin{aligned} \mathcal{M}_s[\gamma^* \rightarrow \gamma + c\bar{c}]|_{pQCD} &= (d_s^{(0)} + d_s^{(\alpha_s)}) \langle c\bar{c} | \mathcal{O}^{c\bar{c}}(^1S_0^{[1]}) | 0 \rangle + (d_s^{(v^2)} + d_s^{(\alpha_s v^2)}) \langle c\bar{c} | \mathcal{P}^{c\bar{c}}(^1S_0^{[1]}) | 0 \rangle \\ &= \sqrt{2N_c} 2E_q [(d_s^{(0)} + d_s^{(\alpha_s)}) + \mathbf{q}^2 (d_s^{(v^2)} + d_s^{(\alpha_s v^2)} + d_s^{(self.)})]. \\ \mathcal{M}_t[\gamma^* \rightarrow \gamma + c\bar{c}]|_{pQCD} &= (d_t^{(0)} + d_t^{(\alpha_s)}) \langle c\bar{c} | \mathcal{O}^{c\bar{c}}(^3P_J^{[1]}) | 0 \rangle + (d_t^{(v^2)} + d_t^{(\alpha_s v^2)}) \langle c\bar{c} | \mathcal{P}^{c\bar{c}}(^3P_J^{[1]}) | 0 \rangle \\ &= \sqrt{2N_c} 2E_q [|\mathbf{q}| (d_t^{(0)} + d_t^{(\alpha_s)}) + \mathbf{q}^3 (d_t^{(v^2)} + d_t^{(\alpha_s v^2)} + d_t^{(self.)})], \end{aligned} \quad (2.13)$$

where \mathcal{M}_s and \mathcal{M}_t represent the amplitudes with the $c\bar{c}$ pair coupling to spin-singlet and spin-triplet polarization, respectively. The above NRQCD operators \mathcal{O} and \mathcal{P} are respectively

defined as follows:

$$\begin{aligned}
\mathcal{O}^{c\bar{c}}(^1S_0^{[1]}) &= \psi^\dagger \chi, \\
\mathcal{P}^{c\bar{c}}(^1S_0^{[1]}) &= \psi^\dagger \left(-\frac{i}{2} \overleftrightarrow{\mathbf{D}}\right)^2 \chi, \\
\mathcal{O}^{c\bar{c}}(^3P_0^{[1]}) &= \frac{1}{3} \psi^\dagger \left(\frac{-i}{2} \overleftrightarrow{\mathbf{D}} \cdot \sigma\right) \chi, \\
\mathcal{P}^{c\bar{c}}(^3P_0^{[1]}) &= \frac{1}{3} \psi^\dagger \left[\left(-\frac{i}{2} \overleftrightarrow{\mathbf{D}}\right)^2 \left(\frac{-i}{2} \overleftrightarrow{\mathbf{D}} \cdot \sigma\right)\right] \chi, \\
\mathcal{O}^{c\bar{c}}(^3P_1^{[1]}) &= \frac{1}{2} \psi^\dagger \left(\frac{-i}{2} \overleftrightarrow{\mathbf{D}} \times \sigma\right) \chi, \\
\mathcal{P}^{c\bar{c}}(^3P_1^{[1]}) &= \frac{1}{2} \psi^\dagger \left[\left(-\frac{i}{2} \overleftrightarrow{\mathbf{D}}\right)^2 \left(\frac{-i}{2} \overleftrightarrow{\mathbf{D}} \times \sigma\right)\right] \chi, \\
\mathcal{O}^{c\bar{c}}(^3P_2^{[1]}) &= \psi^\dagger \left(\frac{-i}{2} \overleftrightarrow{D}^{(i} \sigma^{j)}\right) \chi, \\
\mathcal{P}^{c\bar{c}}(^3P_2^{[1]}) &= \psi^\dagger \left[\left(-\frac{i}{2} \overleftrightarrow{\mathbf{D}}\right)^2 \left(\frac{-i}{2} \overleftrightarrow{D}^{(i} \sigma^{j)}\right)\right] \chi,
\end{aligned} \tag{2.14}$$

where Pauli spinors ψ and χ describe the quark annihilation and the anti-quark creation, respectively. The gauge-covariant derivative operator $\overleftrightarrow{\mathbf{D}} = \overrightarrow{\mathbf{D}} - \overleftarrow{\mathbf{D}}$. The term $d^{(self.)}$ originates from the one-loop self-energy corrections to the NRQCD matrix elements[1, 36, 63, 64] and in the \overline{MS} scheme

$$\langle c\bar{c} | \mathcal{O}^{c\bar{c}} | 0 \rangle_{\overline{MS}} = (\langle c\bar{c} | \mathcal{O}^{c\bar{c}} | 0 \rangle)^{(0)} + \frac{2\alpha_s}{3\pi m_Q^2} C_F \frac{N_\epsilon}{\epsilon_{IR}} (\langle c\bar{c} | \mathcal{P}^{c\bar{c}} | 0 \rangle)^{(0)}, \tag{2.15}$$

where $N_\epsilon(m_Q) \equiv \left(\frac{4\pi\mu_r^2}{m_Q^2}\right)^\epsilon \Gamma(1+\epsilon)$. μ_r is the renormalization scale. Therefore,

$$d^{(self.)} = \frac{2\alpha_s}{3\pi m_Q^2} C_F \left[\frac{1}{\epsilon_{IR}} + \ln 4\pi - \gamma_E + \ln\left(\frac{\mu_r^2}{m_Q^2}\right) \right] d^{(0)}. \tag{2.16}$$

This expression is satisfied for all $^1S_0^{[1]}$ and $^3P_J^{[1]}$ states. Therefore, $d^{(self.)}$ contributes to the amplitudes expansion for $\mathcal{O}(\alpha_s v^2)$. The factor $\sqrt{2N_c}2E_q$ in Eq.(2.13) originates from the perturbative calculations on the LO $Q\overline{Q}$ NRQCD matrix elements. The extra factor $|\mathbf{q}|$ arises from the derivative operator for the P -wave NRQCD operator \mathcal{P} .

The covariant projection method is adopted to calculate the full QCD amplitudes as,

$$\begin{aligned}
\mathcal{M}_s[\gamma^* \rightarrow \gamma + c\bar{c}] &= Tr\{\mathcal{M}[\gamma^* \rightarrow \gamma + c + \bar{c}] \otimes \mathcal{P}_{00} \otimes \pi_1\}, \\
\mathcal{M}_t[\gamma^* \rightarrow \gamma + c\bar{c}] &= Tr\{\mathcal{M}[\gamma^* \rightarrow \gamma + c + \bar{c}] \otimes \mathcal{P}_{1sz} \otimes \pi_1\},
\end{aligned} \tag{2.17}$$

The color-singlet projection operators are defined as $\pi_1 = \mathbf{1}/\sqrt{N_c}$. The spin-singlet and spin-triplet projection operators are given as,

$$\begin{aligned}
\mathcal{P}_{00} &= \frac{1}{2\sqrt{2}(E_q + m_c)} (\not{\epsilon}_{\bar{c}} - m_c) \frac{(-\not{p} + 2E_q)\gamma_5(\not{p} + 2E_q)}{8E_q^2} (\not{p}_c + m_c), \\
\mathcal{P}_{1sz}(\epsilon_s) &= \frac{1}{2\sqrt{2}(E_q + m_c)} (\not{\epsilon}_{\bar{c}} - m_c) \frac{(-\not{p} + 2E_q)\not{\epsilon}_s(\not{p} + 2E_q)}{8E_q^2} (\not{p}_c + m_c),
\end{aligned} \tag{2.18}$$

where \mathcal{P}_{00} and \mathcal{P}_{1s_z} for the spin-singlet and spin-triplet states, respectively. These operators can be expanded up to the \mathbf{q}^2/m_c^2 order applied with Eqs:(2.1),(2.2),(2.4).

According to the matching expression Eq.(2.13), the short-distance coefficients are calculated by

$$\begin{aligned}
d_s^{(0)} &= \frac{\mathcal{M}_s^{(0)}}{\sqrt{2N_c}2m_c}|_{q \rightarrow 0}, \\
d_s^{(\alpha_s)} &= \frac{\mathcal{M}_s^{(\alpha_s)}}{\sqrt{2N_c}2m_c}|_{q \rightarrow 0}, \\
d_s^{(v^2)} &= \frac{1}{2!} \frac{\partial^2}{\partial \mathbf{q}^2} \frac{\mathcal{M}_s^{(0)}}{\sqrt{2N_c}2E_q}|_{q \rightarrow 0}, \\
d_s^{(\alpha_s v^2)} &= \frac{1}{2!} \frac{\partial^2}{\partial \mathbf{q}^2} \frac{\mathcal{M}_s^{(\alpha_s)}}{\sqrt{2N_c}2E_q} - d_s^{self.}|_{q \rightarrow 0}, \\
d_t^{(0)} &= \epsilon_L^{(0)} \frac{\partial}{\partial |\mathbf{q}|} \frac{\mathcal{M}_t^{(0)}}{\sqrt{2N_c}2E_q}|_{q \rightarrow 0}, \\
d_t^{(\alpha_s)} &= \epsilon_L^{(0)} \frac{\partial}{\partial |\mathbf{q}|} \frac{\mathcal{M}_t^{(\alpha_s)}}{\sqrt{2N_c}2E_q}|_{q \rightarrow 0}, \\
d_t^{(v^2)} &= \epsilon_L^{(0)} \frac{1}{3!} \frac{\partial^3}{\partial \mathbf{q}^3} \frac{\mathcal{M}_t^{(0)}}{\sqrt{2N_c}2E_q} + \epsilon_L^{(2)} \frac{d_t^{(0)}}{m_c^2}|_{q \rightarrow 0}, \\
d_t^{(\alpha_s v^2)} &= \epsilon_L^{(0)} \frac{1}{3!} \frac{\partial^3}{\partial \mathbf{q}^3} \frac{\mathcal{M}_t^{(\alpha_s)}}{\sqrt{2N_c}2E_q} + \epsilon_L^{(2)} \frac{d_t^{(\alpha_s)}}{m_c^2} - d_t^{self.}|_{q \rightarrow 0},
\end{aligned} \tag{2.19}$$

where $\mathcal{M}^{(0)}$ and $\mathcal{M}^{(\alpha_s)}$ are defined by the born and one-loop amplitudes, respectively. The replacements are applied to resolve the expansion to the Lorentz vector q in the amplitude expressions:

$$q_\mu q_\nu \rightarrow \frac{\mathbf{q}^2}{D-1} \Pi_{\mu\nu}^{(0)}, \tag{2.20}$$

for S -wave states and

$$q_\mu q_\nu q_\rho \rightarrow \frac{\mathbf{q}^3}{D+1} \{ \Pi_{\mu\nu}^{(0)} [\epsilon_L^{(0)}]_\rho + \Pi_{\mu\rho}^{(0)} [\epsilon_L^{(0)}]_\mu + \Pi_{\nu\rho}^{(0)} [\epsilon_L^{(0)}]_\mu \}, \tag{2.21}$$

for P -wave states.

2.3 One-loop computation

The one-loop Feynman diagrams are shown in Fig.1. The dimensional regularization scheme is selected here. The ultraviolet divergences in one-loop amplitude are canceled by the counterterms. The infrared divergences at the α_s order in one-loop amplitude are also canceled by the counterterm amplitude, and the additional infrared divergences at the order of $\alpha_s v^2$ are canceled by the one-loop self-energy contribution to the NRQCD matrix elements in Eq.2.15

and Eq.2.16. The real corrections need not to be included for the exclusive processes. We apply the method in Ref.[83] to reduce the tensor integration. The relativistic expansion is done before dealing with the loop integrand. The on-mass-shell(OS) renormalization scheme is adopted and in this scheme the renormalization constants are chosen as

$$\begin{aligned}\delta Z_2^{OS} &= -C_F \frac{\alpha_s}{4\pi} N_\epsilon \left(\frac{1}{\epsilon_{UV}} + \frac{2}{\epsilon_{IR}} + 4 \right), \\ \delta Z_{m_Q}^{OS} &= -C_F \frac{\alpha_s}{4\pi} N_\epsilon \left(\frac{3}{\epsilon_{UV}} + 4 \right),\end{aligned}\tag{2.22}$$

where $N_\epsilon(m_Q)$ has been previously defined and the renormalization scale μ_r is canceled by the loop and counterterm diagrams up to the order of $\mathcal{O}(\alpha_s v^2)$. In the OS scheme, the diagrams for the external leg correction are not included. In our calculations, the 't Hooft-Veltman (HV) regularization scheme[94, 95] is adopted in which γ^5 is defined as

$$\gamma^5 \equiv i\gamma^0\gamma^1\gamma^2\gamma^3 = -\frac{i}{4!}\epsilon^{\mu\nu\rho\sigma}\gamma_\mu\gamma_\nu\gamma_\rho\gamma_\sigma,\tag{2.23}$$

The traces involving more than four Dirac γ -matrices with a γ^5 are evaluated recursively by the West Mathematica programs[96]. Our strategy handling of γ^5 is same as that in Ref.[63]. In the HV scheme, the Ward identities may be violated in the one-loop calculations, such as for the axial current known as the Adler-Bell-Jackiw anomalies, which arising from the symmetry breaking of γ_5 definitions in D-dimension as Eq.2.23. In our case, $\gamma^* \rightarrow \gamma\eta_c$ process, for γ_5 appears outside of one-loop integrals, the amplitudes would satisfy the ward identities, that is seen as the short-distance results given in Eq.2.24 in the next section. More discussions of γ^5 -scheme and the anomalous Ward identities could be referred to Refs.[63, 91, 92, 94–99].

We use the `FeynArts`[84] package to generate Feynman diagrams and amplitudes, and the `FeynCalc`[85, 86] package and our self-written `Mathematica` package to handle the amplitudes and the phase space integrand.

2.4 Matching results for η_c

This subsection presents the matching results for the short-distance coefficients for η_c .

The final matching results of the coefficients are given in the Appendix, where $r \equiv 4m_c^2/s$ and s is the square of beam energy. The coefficients are given as follows ¹:

$$\begin{aligned}d_s^{(0)} &= A^{(0)}\epsilon_1, \\ d_s^{(v^2)} &= A^{(v^2)}\epsilon_1 + A^{(0)}\epsilon_2/m_c^2, \\ d_s^{(\alpha_s)} &= A^{(\alpha_s)}\epsilon_1, \\ d_s^{(\alpha_s v^2)} &= A^{(\alpha_s v^2)}\epsilon_1 + A^{(\alpha_s)}\epsilon_2/m_c^2,\end{aligned}\tag{2.24}$$

¹Here, we omit the third term of the coefficients in the orders of v^2 and $\alpha_s v^2$ as shown in the appendix to dilute the contribution of the relativistic renormalization in Eq.(2.12)[30]. In other words, the below coefficients include the contributions of the relativistic renormalization.

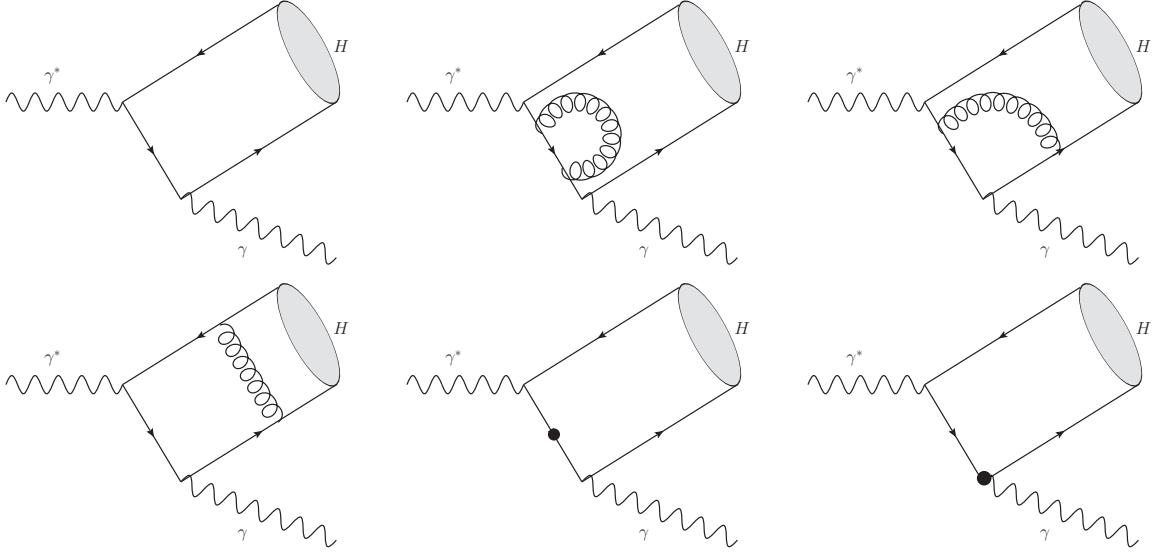


Figure 1. The typical born, loop, and counterterm Feynman diagrams. There are two diagrams for the born amplitude, six diagrams for the counterterm amplitude, and eight for the one-loop amplitude including two self-energy diagrams, four triangle diagrams, and two box diagrams.

where

$$\begin{aligned}\epsilon_1 &\equiv \epsilon^{\mu\nu\rho\tau}(\epsilon_Q^*)_\mu(\epsilon_k^*)_\nu k_\rho^{(0)} p_\tau^{(0)}, \\ \epsilon_2 &\equiv \epsilon_1^{(2)} = \epsilon^{\mu\nu\rho\tau}(\epsilon_Q^*)_\mu(\epsilon_k^*)_\nu(p^{(0)} + k^{(0)})_\rho p_\tau^{(2)},\end{aligned}\tag{2.25}$$

where ϵ_Q and ϵ_k represent the polarization vector of the initial virtual photon and the final photon, respectively.

The coefficients in Eq.(2.24) are provided in the high-energy region. In the limit $r \rightarrow 0$, the asymptotic behavior of these coefficients can be obtained. The lowest order of the coefficients is $\mathcal{O}(r)$; the higher-order contributions are omitted, and the reduced equations are given as follows:

$$\begin{aligned}d_s^{(0)} &= C r \epsilon_1, \\ d_s^{(v^2)} &= -\frac{5}{12m_c^2} C r \epsilon_1, \\ d_s^{(\alpha_s)} &= -\frac{C r \alpha_s \epsilon_1}{9\pi} [3(3 - 2 \ln 2) \ln r + 9(\ln^2 2 - 3 \ln 2 + 3) + \pi^2] \\ &\approx -\frac{C r \alpha_s \epsilon_1 (-4.8 \ln r - 22.5)}{9\pi}, \\ d_s^{(\alpha_s v^2)} &= \frac{C r \alpha_s \epsilon_1}{108m_c^2 \pi} [3(27 - 10 \ln 2) \ln r + (45 \ln^2 2 - 75 \ln 2 - 79) + 5\pi^2] \\ &\approx -\frac{C r \alpha_s \epsilon_1 (5.0 \ln r - 5.0)}{9\pi m_c^2},\end{aligned}\tag{2.26}$$

where $C \equiv \frac{(4\pi\alpha)Q_c^2}{2m_c^3}$. The terms of ϵ_2 disappear in the expressions because ϵ_2 is suppressed by a factor of r than ϵ_1 . The asymptotic behavior of $d^{(\alpha_s)}$ is consistent with that in Ref.[70].

The asymptotic behavior of the coefficients for $r \rightarrow \infty$ corresponds to the process $\eta_c \rightarrow 2\gamma$ are mentioned in Ref.[70] and given as follows²:

$$\begin{aligned}\lim_{r \rightarrow \infty} A^{(0)} &= -C, \\ \lim_{r \rightarrow \infty} A^{(v^2)} &= \frac{17}{12m_c^2}C, \\ \lim_{r \rightarrow \infty} A^{(\alpha_s)} &= \frac{C\alpha_s(20 - \pi^2)}{6\pi}, \\ \lim_{r \rightarrow \infty} A^{(\alpha_s v^2)} &= \frac{C\alpha_s}{216m_c^2\pi}(384 \ln 2 - 844 + 63\pi^2).\end{aligned}\tag{2.27}$$

Note that,

$$\lim_{r \rightarrow \infty} \epsilon_2 = \epsilon^{\mu\nu\rho\tau}(\epsilon_Q^*)_\mu(\epsilon_k^*)_\nu(k_\rho^{(2)}p_\tau^{(0)} + k_\rho^{(0)}p_\tau^{(2)}) = \epsilon_1.\tag{2.28}$$

Therefore, the NLO short-distance coefficients in v^2 are given by

$$\begin{aligned}\lim_{r \rightarrow \infty} d_s^{(v^2)} &= \frac{5C}{12m_c^2}\epsilon_1 = -\frac{5}{12m_c^2}\lim_{r \rightarrow \infty} d^{(0)}, \\ \lim_{r \rightarrow \infty} d_s^{(\alpha_s v^2)} &= \frac{C\alpha_s}{m_c^2\pi}\left(\frac{16 \ln 2}{9} - \frac{31}{54} + \frac{\pi^2}{8}\right).\end{aligned}\tag{2.29}$$

The short-distance in $\mathcal{O}(\alpha_s v^2)$ is consistent with Ref.[63] if we disregard the contribution of the relativistic renormalization in Eq.(2.12) which contributes a factor of 1/4.

2.5 Matching results for χ_{cJ}

This subsection presents the matching results for the short-distance coefficients for χ_{cJ} .

Similar to the η_c case, the short-distance coefficients in the orders of v^2 and $\alpha_s v^2$ for χ_{cJ} are also written in two parts. All the coefficients are given as follows:

$$\begin{aligned}d_t^{(0)} &= B^{(0)}\epsilon_3, \\ d_t^{(v^2)} &= B^{(v^2)}\epsilon_3 + B^{(0)}\epsilon_4/m_c^2, \\ d_t^{(\alpha_s)} &= B^{(\alpha_s)}\epsilon_3, \\ d_t^{(\alpha_s v^2)} &= B^{(\alpha_s v^2)}\epsilon_3 + B^{(\alpha_s)}\epsilon_4/m_c^2,\end{aligned}\tag{2.30}$$

where

$$\begin{aligned}\epsilon_3 &\equiv (\epsilon_Q^*)_\mu(\epsilon_k^*)_\nu \mathcal{P}_{\alpha\beta}^{(0)}, \\ \epsilon_4 &\equiv (\epsilon_Q^*)_\mu(\epsilon_k^*)_\nu \mathcal{P}_{\alpha\beta}^{(2)}.\end{aligned}\tag{2.31}$$

²Comparing of the previous results of the $\mathcal{O}(v^2)$ corrections with the di-photon decay process for η_c and χ_c [1, 82, 87], we find that the absolute values of our results differ by 1/4 which originates from the relativistic renormalization expansion (Eq.2.12). Therefore the coefficients of the relativistic corrections for the η_c , χ_c decay widths shown in Tab.3 differ by 1/2 from the previous works.

The asymptotic behavior in the limit $r \rightarrow 0$ is also considered. For the ϵ_4 is higher order than ϵ_3 in r , then the coefficients are given as follows:

$$\begin{aligned}
\lim_{r \rightarrow 0} d_t^{(0)} &= D\epsilon_3(g^{\alpha\nu}g^{\beta\mu} - g^{\alpha\mu}g^{\beta\nu}), \\
\lim_{r \rightarrow 0} d_t^{(v^2)} &= -\frac{D\epsilon_3}{20m_c^2}(11g^{\alpha\nu}g^{\beta\mu} - 11g^{\alpha\mu}g^{\beta\nu} + 2g^{\alpha\beta}g^{\mu\nu}), \\
\lim_{r \rightarrow 0} d_t^{(\alpha_s)} &= \frac{D\alpha_s\epsilon_3}{9\pi} \left\{ (g^{\alpha\nu}g^{\beta\mu} - g^{\alpha\mu}g^{\beta\nu})[3(3 - 2\ln 2)\ln r + 3(3\ln^2 2 - 5\ln 2 + 7)\pi^2] \right. \\
&\quad \left. + 6g^{\alpha\beta}g^{\mu\nu}(1 + 2\ln 2) \right\}, \\
\lim_{r \rightarrow 0} d_t^{(\alpha_s v^2)} &= \frac{D\alpha_s\epsilon_3}{540\pi m_c^2} \left\{ 6g^{\alpha\beta}g^{\mu\nu}[3(1 - 2\ln 2)\ln r + (9\ln^2 2 - 99\ln 2 - 93) + \pi^2] \right. \\
&\quad \left. + (g^{\alpha\nu}g^{\beta\mu} - g^{\alpha\mu}g^{\beta\nu})[9(45 - 22\ln 2)\ln r + (297\ln^2 2 - 75\ln 2 - 77 + 33\pi^2)] \right\}.
\end{aligned} \tag{2.32}$$

3 Cross section

The cross sections of the process $e^+e^- \rightarrow \gamma H$ are relative to the squared amplitudes of the process $\gamma^* \rightarrow \gamma H$,

$$\sigma(e^+e^- \rightarrow \gamma H) = \frac{1}{2s} \frac{2(D-2)(4\pi\alpha)}{(D-1)s} \int \Phi_2 \overline{\sum} |\mathcal{M}(\gamma^* \rightarrow \gamma H)|^2. \tag{3.1}$$

$\overline{\sum}$ means obtaining the sum of NRQCD amplitudes \mathcal{M} over the final-state color and polarization and the average over the ones of the initial states. Where the differential two-body phase space in D dimensions can be solved:

$$\begin{aligned}
\int \Phi_2 &= \frac{1}{8\pi} \left(\frac{4\pi}{s}\right)^\epsilon \left(1 - \frac{M_H^2}{s}\right)^{1-2\epsilon} \frac{\Gamma(1-\epsilon)}{\Gamma(2-2\epsilon)} \\
&\approx \frac{1}{8\pi} \left(\frac{4\pi}{s}\right)^\epsilon (1-r)^{1-2\epsilon} \left[1 - \frac{r(1-2\epsilon)}{1-r} \frac{\mathbf{q}^2}{m_c^2}\right] \frac{\Gamma(1-\epsilon)}{\Gamma(2-2\epsilon)},
\end{aligned} \tag{3.2}$$

where $M_H \approx 2E_q$ has been chosen. This expression implies that the two-body phase space contributes another factor of $-r/(1-r)$ to the v^2 order cross section. This factor is linearly divergent near the low-energy threshold.

The results of short-distance amplitudes are obtained in the last section. Then the cross sections for η_c and χ_{cJ} states can be obtained as follows:

$$\sigma = \hat{\sigma}^{(0)} [1 + \alpha_s c^{10} + (c^{02} + \alpha_s c^{12}) \langle v^2 \rangle] \langle 0 | \mathcal{O}^H | 0 \rangle, \tag{3.3}$$

where $\hat{\sigma}^{(0)}$ is the LO short-distance cross section, and the matrix element $\langle v^2 \rangle$ is defined as follows:

$$\langle v^2 \rangle \equiv \frac{\langle 0 | \mathcal{P}^H | 0 \rangle}{m_c^2 \langle 0 | \mathcal{O}^H | 0 \rangle}. \tag{3.4}$$

3.1 η_c

The LO short-distance cross section for η_c is given by:

$$\hat{\sigma}_{\eta_c}^{(0)} = \frac{(4\pi\alpha)^3 Q_c^4 (1-r)}{6\pi m_c s^2}. \quad (3.5)$$

Fig.2 shows that the radios c^{10} , c^{02} , and c^{11} ranging r from 0 to 0.5, ie. high-energy to low-energy, for η_c production. The $\mathcal{O}(\alpha_s v^2)$ correction is suppressed by $\alpha_s \langle v^2 \rangle$ and negligibly contributes to the total cross section at the $r = 0.5$. Tab.1 presents the asymptotic behaviors of the radios near the threshold. The radio c^{12} for the $\mathcal{O}(\alpha_s v^2)$ correction is about $4.8/\pi$ if the corrections from the phase space are not considered, the $\mathcal{O}(\alpha_s v^2)$ contribution without the phase space contribution is one fifth of the $\mathcal{O}(\alpha_s)$ contribution near the threshold if $\langle v^2 \rangle = 0.2$. The phase space brings an additional linear singularity factor that markedly enhances the $\mathcal{O}(v^2)$ and $\mathcal{O}(\alpha_s v^2)$ contributions. However, the total coefficient of the singularity $1/(1-r)$ is $(4\alpha_s/\pi - 1)\langle v^2 \rangle$ and there is a negative residue singularity. The $\mathcal{O}(\alpha_s v^2)$ corrections becomes significant at the high-energy region and provides negative contributions under the same sign with the $\mathcal{O}(v^2)$ and $\mathcal{O}(\alpha_s)$ ones as Tab.2. For the B factories energy region ($r \approx 0.07$), the contributions from $\mathcal{O}(\alpha_s v^2)$ corrections are numerically suppressed by $\langle v^2 \rangle$ than those from $\mathcal{O}(\alpha_s)$ corrections.

Tab.3 lists the corresponding coefficients for the decay process $\eta_c \rightarrow \gamma\gamma$. The $\mathcal{O}(\alpha_s v^2)$ contribution slightly affects the decay rate, although our numerically calculated value is slightly larger than that from Ref.[63]. However, the $\mathcal{O}(\alpha_s v^2)$ contribution can re-determine the elements $\langle v^2 \rangle$ for the color-singlet S -wave states.

Table 1. The asymptotic behaviors of the radios near the threshold. The radios are defined in Eq.(3.3). The last term in each cell of c^{02} and c^{12} originates from the phase space corrections.

	$\lim_{r \rightarrow 1} c^{02}$	$\lim_{r \rightarrow 1} c^{10}$	$\lim_{r \rightarrow 1} c^{12}$
η_c	$-\frac{5}{6} - \frac{1}{1-r}$	$-\frac{4}{\pi}$	$\frac{130}{27\pi} + \frac{4}{\pi(1-r)}$
χ_{c0}	$\frac{2}{1-r} - \frac{11}{10} - \frac{1}{1-r}$	$-\frac{16}{3\pi}$	$-\frac{32}{3\pi(1-r)} + \frac{160 \ln[2(1-r)] - 166}{45\pi} + \frac{16}{3\pi(1-r)}$
χ_{c1}	$\frac{2}{1-r} - \frac{13}{5} - \frac{1}{1-r}$	$-\frac{16}{3\pi}$	$-\frac{32}{3\pi(1-r)} + \frac{160 \ln[2(1-r)] + 389}{45\pi} + \frac{16}{3\pi(1-r)}$
χ_{c2}	$\frac{2}{1-r} - 2 - \frac{1}{1-r}$	$-\frac{16}{3\pi}$	$-\frac{32}{3\pi(1-r)} + \frac{160 \ln[2(1-r)] + 131}{45\pi} + \frac{16}{3\pi(1-r)}$

3.2 χ_{cJ}

The LO short-distance cross section for χ_{cJ} is calculated as

$$\begin{aligned} \hat{\sigma}_{\chi_{c0}}^{(0)} &= \frac{(4\pi\alpha)^3 Q_c^4 (1-3r)^2}{18\pi m_c^3 s^2 (1-r)}, \\ \hat{\sigma}_{\chi_{c1}}^{(0)} &= \frac{(4\pi\alpha)^3 Q_c^4 (1+r)}{3\pi m_c^3 s^2 (1-r)}, \\ \hat{\sigma}_{\chi_{c2}}^{(0)} &= \frac{(4\pi\alpha)^3 Q_c^4 (1+3r+6r^2)}{9\pi m_c^3 s^2 (1-r)}, \end{aligned} \quad (3.6)$$

Table 2. The asymptotic behaviors of the radii in the high-energy limit. The radii are defined in Eq.(3.3). The asymptotic results for c^{10} are consistent with Ref.[70] and for c^{02} are consistent with Ref.[72].

η_c	$\lim_{r \rightarrow 0} c^{02} = -\frac{5}{6}$
	$\lim_{r \rightarrow 0} c^{10} = -\frac{2}{9\pi}[3(3 - 2 \ln 2) \ln r + 9(\ln^2 2 - 3 \ln 2 + 3) + \pi^2]$ $\approx -0.34 \ln r - 1.59$
	$\lim_{r \rightarrow 0} c^{12} = \frac{1}{27\pi}[3(21 - 10 \ln 2) \ln r + 15(3 \ln^2 2 - 7 \ln 2) + 28 + 5\pi^2]$ $\approx 0.50 \ln r + 0.31$
χ_{c0}	$\lim_{r \rightarrow 0} c_{\chi_{c0}}^{02} = -\frac{13}{10}$
	$\lim_{r \rightarrow 0} c_{\chi_{c0}}^{10} = -\frac{2}{9\pi}[3(1 - 2 \ln 2) \ln r + 3 \ln 2(3 \ln 2 - 11) + \pi^2]$ $\approx 0.08 \ln r + 0.61$
	$\lim_{r \rightarrow 0} c_{\chi_{c0}}^{12} = \frac{1}{135\pi}[9(23 - 26 \ln 2) \ln r + 3 \ln 2(117 \ln 2 - 443) - 637 + 39\pi^2]$ $\approx 0.11 \ln r - 2.37$
χ_{c1}	$\lim_{r \rightarrow 0} c_{\chi_{c1}}^{02} = -\frac{11}{10}$
	$\lim_{r \rightarrow 0} c_{\chi_{c1}}^{10} = -\frac{2}{9\pi}[3(3 - 2 \ln 2) \ln r + 3 \ln 2(3 \ln 2 - 5) + 21 + \pi^2]$ $\approx -0.34 \ln r - 1.75$
	$\lim_{r \rightarrow 0} c_{\chi_{c1}}^{12} = \frac{1}{135\pi}[9(39 - 22 \ln 2) \ln r + 3 \ln 2(99 \ln 2 - 95) - 637 + 33\pi^2]$ $\approx 0.50 \ln r + 1.36$
χ_{c2}	$\lim_{r \rightarrow 0} c_{\chi_{c2}}^{02} = -\frac{7}{10}$
	$\lim_{r \rightarrow 0} c_{\chi_{c2}}^{10} = -\frac{2}{9\pi}[3(1 - 2 \ln 2) \ln r + 3 \ln 2(3 \ln 2 + 1) + 18 + \pi^2]$ $\approx 0.08 \ln r - 2.42$
	$\lim_{r \rightarrow 0} c_{\chi_{c2}}^{12} = \frac{1}{135\pi}[9(17 - 14 \ln 2) \ln r + 3 \ln 2(63 \ln 2 + 79) + 389 + 21\pi^2]$ $\approx 0.15 \ln r + 2.00$

Table 3. The asymptotic behaviors of the radii in the limit of $r \rightarrow \infty$. The radii are defined in Eq.(3.3). These results are corresponding the radii of the two-photon decay rates for η_c , χ_{c0} and χ_{c2} . $\chi_{c1} \rightarrow 2\gamma$ is forbade therefore the radii are not given for it.

	$\lim_{r \rightarrow \infty} c^{02}$	$\lim_{r \rightarrow \infty} c^{10}$	$\lim_{r \rightarrow \infty} c^{12}$
η_c	$-\frac{5}{6} \approx -0.83$	$\frac{1}{3\pi}[\pi^2 - 20] \approx -1.1$	$-\frac{1}{54\pi}[192 \ln 2 + 21\pi^2 - 212] \approx -0.8$
χ_{c0}	$-\frac{11}{6} \approx -1.83$	$\frac{1}{9\pi}[3\pi^2 - 28] \approx -0.06$	$-\frac{1}{90\pi}[320 \ln 2 + 65\pi^2 - 196] \approx -2.36$
χ_{c2}	$-\frac{3}{2} = -1.5$	$-\frac{16}{3\pi} \approx -1.7$	$-\frac{1}{135\pi}[48 \ln 2 - 9\pi^2 - 1148] \approx 2.8$

For χ_{c0} , the radii may be divergent at $r = 1/3$ for the LO short-distance coefficient reach zero at this point as Eq.(3.6). Thus, we change Eq.(3.3) into the following formula to

define the radios:

$$\sigma_{\chi_{c0}} = \frac{(4\pi\alpha)^3 Q_c^4}{18\pi m_c^3 s^2} [c^{00} + \alpha_s c^{10} + (c^{02} + \alpha_s c^{12}) \langle v^2 \rangle] \langle 0 | \mathcal{O}^H | 0 \rangle. \quad (3.7)$$

The redefined radios are shown as Fig.3 and these radios are proportional to the relative short-distance cross sections. By a rough estimation, the LO cross sections are diluted by the sum of the $\mathcal{O}(\alpha_s)$ and $\mathcal{O}(v^2)$ corrections as shown in figure. Furthermore, the $\mathcal{O}(\alpha_s v^2)$ contributes additional negative corrections. Thus, the total cross sections for the χ_{c0} process may be small.

The radios for χ_{c1} and χ_{c2} processes are shown in Fig.4 and Fig.5, respectively. In the low-energy region ($0.3 < r < 0.5$), the $\mathcal{O}(\alpha_s v^2)$ corrections contribute the most. Meanwhile the $\mathcal{O}(v^2)$ and $\mathcal{O}(\alpha_s v^2)$ corrections increase as fast as r , and they have different signs. As shown in Tab.1, the behaviors of the radios are similar for all the P -wave states. The radio c^{02} for the $\mathcal{O}(v^2)$ correction near the threshold has an additional linear singularity $1/(1-r)$ for the LO cross section. The radio c^{10} for the $\mathcal{O}(\alpha_s)$ corrections is a negative constant. In other words, the $\mathcal{O}(\alpha_s)$ contribution has the same rate as the corresponding LO cross section for different χ_{cJ} states. For the $\mathcal{O}(\alpha_s v^2)$ corrections, a logarithmic singularity term $\ln(1-r)$ aside from the linear singularity term also exists. We sum the linear singularity in the $\mathcal{O}(v^2)$ corrections and $\mathcal{O}(\alpha_s v^2)$ corrections and obtain the coefficient of the linear singularity as $(1 - 16\alpha_s/3\pi) \langle v^2 \rangle \approx -0.5 \langle v^2 \rangle$. The coefficient of the residual linear singularity is similar to that of η_c . The linear singularity half originates from the phase space. For the high-energy region, we consider the suppressed factor $\alpha_s \langle v^2 \rangle$ to the $\mathcal{O}(v^2)$ corrections. The numerical results in the high-energy approximation in Tab.2 show that the corrections are much smaller than the α_s and v^2 corrections.

The radios corresponding to the two-photon decay for χ_{c0} and χ_{c2} are also given in Tab.3. By the rough estimation, we select α_s and $\langle v^2 \rangle$ as a range of $0.2 \sim 0.3$. Therefore the $\mathcal{O}(\alpha_s v^2)$ corrections contributes $10\% \sim 20\%$ to the LO decay rate for $\chi_{c0} \rightarrow 2\gamma$ or $\chi_{c2} \rightarrow 2\gamma$. These $\mathcal{O}(\alpha_s v^2)$ corrections may also significantly affect fitting to the element $\langle v^2 \rangle$ for χ_{cJ} .

4 Numerical results and discussion

In this section, we revisit the numerical calculations to the cross sections. In our numerical calculation, the total cross sections strongly depend on the input parameters (e.g., mass of the charm quark, long distance matrix elements, and the strong-coupling constant). The relativistic matrix elements can hardly be determined. In the consequent calculations for the $\eta_c(1S)$, $\chi_{cJ}(1P)$ process, we select the fine structure constant $\alpha = 1/137$ and the charm quark mass as

$$m_c = 1.5 \pm 0.1 \text{ GeV}, \quad (4.1)$$

for both the $\eta_c(1S)$ and $\chi_{cJ}(1P)$ process. The strong-coupling constant is chosen as

$$\alpha_s = 0.23 \pm 0.03. \quad (4.2)$$

The matrix elements $\langle v^2 \rangle$ are chosen as ³

$$\begin{aligned}\langle v^2 \rangle^{\eta_c} &= 0.15 \pm 0.1, \\ \langle v^2 \rangle^{\chi_{cJ}} &= 0.20 \pm 0.1,\end{aligned}\tag{4.3}$$

The LO long-distance matrix elements are obtained from the radial wave functions at the origin in the potential model calculations [88] with the replacements

$$\begin{aligned}\langle 0 | \mathcal{O}^{\eta_c(nS)} | 0 \rangle &= \frac{2N_c |R_{nS}(0)|^2}{4\pi}, \\ \langle 0 | \mathcal{O}^{\chi_{c0}(mP)} | 0 \rangle &= \frac{6N_c |R'_{mP}(0)|^2}{4\pi},\end{aligned}\tag{4.4}$$

and

$$\begin{aligned}\langle 0 | \mathcal{O}^{\chi_{cJ}(mP)} | 0 \rangle &= (2J+1)(1 + \mathcal{O}(v^2)) \langle 0 | \mathcal{O}^{\chi_{c0}(mP)} | 0 \rangle \\ &\approx (2J+1) \langle 0 | \mathcal{O}^{\chi_{c0}(mP)} | 0 \rangle.\end{aligned}\tag{4.5}$$

In the last step, we ignore the $\mathcal{O}(v^2)$ term to simplify the input parameters. The results markedly depend on the selections of the wave functions at the origin. Studies in Ref.[69, 73] have adopted two sets of wave functions at the origin with large gaps. We re-estimate the wave functions at the origin by averaging the two sets of wave functions with the uncertainties in Tab.4. The wave functions at the origin for $4S$ and $3P$ states are estimated like Ref.[72] as

Table 4. The wave functions at the origin [88]. The two sets represent the calculations from the Cornell potential and the B-T potential. "Re-est" are averaged from the two sets of functions with the uncertainties.

	$1S(\text{GeV}^3)$	$2S(\text{GeV}^3)$	$3S(\text{GeV}^3)$	$1P(\text{GeV}^5)$	$2P(\text{GeV}^5)$
Cornell	1.454	0.927	0.791	0.131	0.186
B-T	0.81	0.529	0.455	0.075	0.102
Re-est	1.132 ± 0.322	0.728 ± 0.199	0.623 ± 0.168	0.103 ± 0.028	0.144 ± 0.042

$$\begin{aligned}R_{4S} &= 2R_{3S} - R_{2S} = 0.518 \pm 0.391 \text{ GeV}^3, \\ R'_{3P} &= (R'_{1P} + R'_{2P})/2 = 0.124 \pm 0.025 \text{ GeV}^5.\end{aligned}\tag{4.6}$$

³For the P -wave states, we can use our new up to $\mathcal{O}(\alpha_s v^2)$ results for $\chi_{c0} \rightarrow \gamma\gamma$ and $\chi_{c2} \rightarrow \gamma\gamma$ to fit $\langle v^2 \rangle$:

$$\begin{aligned}\Gamma[\chi_{c0} \rightarrow \gamma\gamma] &= \frac{6\pi Q_c^4 \alpha^2}{m_c^4} \langle \mathcal{O}^{\chi_{c0}} \rangle [1 - 0.06\alpha_s - (1.83 + 2.36\alpha_s) \langle v^2 \rangle^{\chi_{c0}} - 3a_8], \\ \Gamma[\chi_{c2} \rightarrow \gamma\gamma] &= \frac{8\pi Q_c^4 \alpha^2}{5m_c^4} \langle \mathcal{O}^{\chi_{c2}} \rangle [1 - 1.7\alpha_s - (1.5 - 2.8\alpha_s) \langle v^2 \rangle^{\chi_{c2}} - 2.3a_8 - 1.7a_F].\end{aligned}$$

The color-octet contributions in the above formula originate from Ref.[87]. In the estimation, we ignore the v^2 corrections to the elements and assume $\langle \mathcal{O}^{\chi_{c2}} \rangle = 5\langle \mathcal{O}^{\chi_{c0}} \rangle$ and $\langle v^2 \rangle^{\chi_c} \equiv \langle v^2 \rangle^{\chi_{c0}} = \langle v^2 \rangle^{\chi_{c2}}$. If we take $a_8 = a_F = 0.1$ then $\langle v^2 \rangle^{\chi_c} = 0.32 \pm 0.04$ is obtained. If we ignore the contributions of the a_8 and a_F terms, then $\langle v^2 \rangle^{\chi_c} = 0.21 \pm 0.03$. Therefore $\langle v^2 \rangle^{\chi_c} = 0.2 \pm 0.1$ are compatible for these results. In this study, we select $\alpha_s = 0.23 \pm 0.03$ and the di-photon decay width for χ_{c0} and χ_{c2} are $(2.23 \pm 0.17) \times 10^{-4} \text{ MeV/c}$ and $(2.59 \pm 0.16) \times 10^{-4} \text{ MeV/c}$, respectively, cited from PDG[80].

In the BESIII energy region, the corrections from the phase space are significant for the cross sections. However, the contributions cannot be determined because of the non-perturbative effects. In the previous works, two different strategies are used to remedy the non-perturbative effects from the phase space integrand, a extra factor is introduced in Ref.[73] and the charm quark mass is set to half of the meson mass in Ref.[72]. Furthermore, as stated in Ref.[32, 89, 90], the v^2 corrections from the phase space, which are related to the terms in the short-distance cross section expansion different with that in the sub-amplitude expansion, could be resummed to all orders in v^2 by the 'shape functions' method. In this paper, we calculate the contributions from the phase space just by a simplified expansion by Eq.(3.2). Therefore, we analyze the cross sections with and without the phase space corrections for comparative and referential purposes.

Tab.5 presents the total cross sections of up to $\alpha_s v^2$ order and the corresponding uncertainties for the η_c process. And Fig.6 presents the corresponding cross sections at the BESIII energy region. The uncertainties for the total cross sections come from the uncertainties of m_c , α_s , $\langle v^2 \rangle$, and the wave functions at the origin. The phase space reduces the numerical results by a factor of 25% \sim 10% and enhances the uncertainties by a factor of 35% \sim 25% in the BESIII energy region 4 \sim 5GeV. The $\mathcal{O}(\alpha_s v^2)$ corrections negligibly contribute to the η_c process. Numerical simulations reveal that these corrections are approximately one-eighth and one-tenth of the $\mathcal{O}(\alpha_s)$ contributions in the energy regions of the B- factories and BESIII, respectively.

Table 5. The total cross sections in fb up to $\alpha_s v^2$ order of $e^+e^- \rightarrow \eta_c(nS) + \gamma$ with $n = 1, 2, 3, 4$ in the BESIII and B-factories energy region. WP and OP indicate considering or ignoring the phase space contributions, respectively. The uncertainties in each cell originate from the uncertainties of the wave functions at the origin, α_s , $\langle v^2 \rangle$, and charm quark mass m_c in turns. For the excited states, we select the charm quark mass as the half of the meson mass in the calculations, therefore there are no m_c uncertainties. The masses of $\eta_c(nS)$ are selected as 3.639GeV, 3.994GeV, and 4.250GeV for $n = 2, 3, 4$ respectively[74, 80].

$\sqrt{s}(\text{GeV})$	4.25	4.50	4.75
1S OP	$1007 \pm 286 \pm 68 \pm 114 \pm 198$	$887 \pm 252 \pm 60 \pm 105 \pm 155$	$775 \pm 220 \pm 52 \pm 95 \pm 123$
1S WP	$832 \pm 237 \pm 57 \pm 231 \pm 209$	$762 \pm 217 \pm 52 \pm 189 \pm 162$	$683 \pm 194 \pm 46 \pm 156 \pm 129$
2S OP	$282 \pm 77 \pm 17 \pm 26$	$284 \pm 77 \pm 18 \pm 29$	$269 \pm 74 \pm 18 \pm 30$
2S WP	$99 \pm 27 \pm 5 \pm 117$	$155 \pm 42 \pm 10 \pm 93$	$176 \pm 48 \pm 12 \pm 76$
3S OP	$101 \pm 27 \pm 5 \pm 7$	$142 \pm 38 \pm 8 \pm 12$	$153 \pm 41 \pm 9 \pm 14$
3S WP	$-74 \pm 20 \pm 5 \pm 95$	$19 \pm 5 \pm 0.4 \pm 73$	$65 \pm 18 \pm 4 \pm 58$
4S OP		$58 \pm 44 \pm 3 \pm 4$	$81 \pm 64 \pm 5 \pm 7$
4S WP		$-52 \pm 39 \pm 4 \pm 59$	$6 \pm 4 \pm 0.1 \pm 46$
$\sqrt{s}(\text{GeV})$	5.00	10.6	11.2
1S OP	$674 \pm 192 \pm 45 \pm 85 \pm 100$	$55 \pm 16 \pm 2 \pm 8 \pm 5$	$45 \pm 13 \pm 2 \pm 7 \pm 4$
1S WP	$607 \pm 173 \pm 41 \pm 130 \pm 103$	$54 \pm 15 \pm 2 \pm 9 \pm 5$	$44 \pm 13 \pm 2 \pm 7 \pm 4$
2S OP	$247 \pm 68 \pm 17 \pm 29$	$25 \pm 7 \pm 1 \pm 4$	$20 \pm 6 \pm 1 \pm 3$
2S WP	$179 \pm 49 \pm 13 \pm 63$	$24 \pm 7 \pm 1 \pm 4$	$20 \pm 5 \pm 1 \pm 4$
3S OP	$151 \pm 41 \pm 10 \pm 16$	$18 \pm 5 \pm 1 \pm 3$	$15 \pm 4 \pm 1 \pm 2$
3S WP	$87 \pm 23 \pm 6 \pm 48$	$18 \pm 5 \pm 1 \pm 3$	$15 \pm 4 \pm 1 \pm 3$
4S OP	$93 \pm 70 \pm 6 \pm 9$	$14 \pm 11 \pm 1 \pm 2$	$12 \pm 9 \pm 1 \pm 2$
4S WP	$36 \pm 27 \pm 2 \pm 37$	$13 \pm 10 \pm 1 \pm 3$	$11 \pm 8 \pm 1 \pm 2$

Tab.6 presents the total cross sections up to $\alpha_s v^2$ order for χ_{c0} process with the uncertainties. The positive $\mathcal{O}(\alpha_s)$ corrections and negative $\mathcal{O}(v^2)$ corrections cancel to each other in the BESIII energy region[72], but $\mathcal{O}(\alpha_s)$ parts also contribute negative corrections which decrease the LO cross sections significantly even to a negative values. And the uncertainties are too large compared with the central values to give a reliable predictions for the χ_{c0} processes in the BESIII energy region.

Table 6. The total cross sections in fb up to $\alpha_s v^2$ order of $e^+e^- \rightarrow \chi_{c0}(nP) + \gamma$ with $n = 1, 2, 3$ in the BESIII and B-factories energy region. WP and OP indicate considering or ignoring the phase space contributions, respectively. The uncertainties in each cell come from the uncertainties of the wave functions at the origin, α_s , $\langle v^2 \rangle$, and charm quark mass m_c in turns. For the excited states, we select the charm quark mass as the half of the meson mass in the calculations, therefore there are no m_c uncertainties. The mass of $\chi_{c0}(nP)$ is selected as 3.918GeV and 4.131GeV for $n = 2, 3$ respectively[74, 80].

$\sqrt{s}(\text{GeV})$	4.25	4.50	4.75
1P OP	$17.4 \pm 4.7 \pm 15.8 \pm 10.8 \pm 39.2$	$-5.1 \pm 1.4 \pm 7.2 \pm 2.2 \pm 13.9$	$-8.8 \pm 2.4 \pm 3.3 \pm 1.0 \pm 4.1$
1P WP	$18.3 \pm 5.0 \pm 13.9 \pm 11.3 \pm 35.8$	$-3.6 \pm 1.0 \pm 6.5 \pm 3.0 \pm 13.6$	$-8.0 \pm 2.2 \pm 3.0 \pm 0.5 \pm 4.5$
2P OP	$2558 \pm 746 \pm 308 \pm 933$	$552 \pm 161 \pm 83 \pm 177$	$170 \pm 49 \pm 32 \pm 51$
2P WP	$1174 \pm 723 \pm 202 \pm 540$	$428 \pm 174 \pm 60 \pm 114$	$141 \pm 58 \pm 25 \pm 37$
3P OP		$1331 \pm 268 \pm 163 \pm 479$	$320 \pm 64 \pm 48 \pm 102$
3P WP		$932 \pm 188 \pm 108 \pm 280$	$248 \pm 50 \pm 35 \pm 66$
$\sqrt{s}(\text{GeV})$	5.00	10.6	11.2
1P OP	$-7.3 \pm 2.0 \pm 1.4 \pm 2.2 \pm 0.$	$1.6 \pm 0.4 \pm 0. \pm 0.5 \pm 0.4$	$1.4 \pm 0.4 \pm 0. \pm 0.4 \pm 0.3$
1P WP	$-6.9 \pm 1.9 \pm 1.4 \pm 2.0 \pm 0.5$	$1.6 \pm 0.4 \pm 0. \pm 0.5 \pm 0.4$	$1.3 \pm 0.4 \pm 0. \pm 0.4 \pm 0.3$
2P OP	$58 \pm 17 \pm 15 \pm 18$	$0.7 \pm 0.2 \pm 0. \pm 0.3$	$0.6 \pm 0.2 \pm 0. \pm 0.2$
2P WP	$51 \pm 21 \pm 12 \pm 15$	$0.6 \pm 0.3 \pm 0. \pm 0.3$	$0.6 \pm 0.2 \pm 0. \pm 0.2$
3P OP	$104 \pm 21 \pm 20 \pm 32$	$0.4 \pm 0.1 \pm 0. \pm 0.2$	$0.4 \pm 0.1 \pm 0. \pm 0.2$
3P WP	$87 \pm 17 \pm 15 \pm 23$	$0.4 \pm 0.1 \pm 0. \pm 0.2$	$0.4 \pm 0.1 \pm 0. \pm 0.2$

Tab.7 and Tab.8 present the total cross sections up to the $\alpha_s v^2$ order for the χ_{c1} and χ_{c2} processes, respectively, with the uncertainties. In the BESIII energy region, they exhibit similar trends. In addition, Fig.7 and Fig.8 show that the total cross sections for χ_{c2} decrease slightly faster than those for χ_{c1} as the energy increase. The $\mathcal{O}(\alpha_s v^2)$ contributions are in behalf of the $\mathcal{O}(v^2)$ ones in this region as discussed in Sec.3. The phase space corrections reduce the total cross sections by a factor of 10% \sim 20% in the BESIII energy region for both the χ_{c0} and χ_{c1} processes. The corresponding uncertainties markedly decrease. From the tables, the χ_{c1} and χ_{c2} states will be found in the BESIII energy region even if the lower bound of the numerical values is adopted for the cross sections.

For the high $\eta_c(ns)$ and $\chi_{cJ}(nP)$ states, the masses of these states extremely approximate the BESIII beam energy. NRQCD factorization will be broken down near the endpoint. In our previous works by Ref.[72], the charm quark mass is set the half of the meson. But in Ref[69, 73], different strategy is used to remedy the phase space integrand near the threshold, an additional unitary factor is introduced, and the charm quark mass is set about 1.5 GeV.

Table 7. The total cross sections in fb up to $\alpha_s v^2$ order of $e^+e^- \rightarrow \chi_{c1}(nP) + \gamma$ with $n = 1, 2, 3$ in the BESIII and B-factories energy region. WP and OP indicate considering or ignoring the phase space contributions, respectively. The uncertainties in each cell come from the uncertainties of the wave functions at the origin, α_s , $\langle v^2 \rangle$, and charm quark mass m_c in turns. For the excited states, we select the charm quark mass as the half of the meson mass in the calculations, therefore there are no m_c uncertainties. The mass of $\chi_{c1}(nP)$ is selected as 3.901GeV and 4.178GeV for $n = 2, 3$ respectively[74, 80].

$\sqrt{s}(\text{GeV})$	4.25	4.50	4.75
1P OP	$1716 \pm 466 \pm 185 \pm 151 \pm 86$	$1127 \pm 306 \pm 117 \pm 64 \pm 0.3$	$783 \pm 213 \pm 79 \pm 24 \pm 27$
1P WP	$1435 \pm 390 \pm 156 \pm 11 \pm 25$	$967 \pm 263 \pm 102 \pm 16 \pm 26$	$685 \pm 186 \pm 70 \pm 25 \pm 39$
2P OP	$10456 \pm 3050 \pm 1099 \pm 3524$	$3374 \pm 984 \pm 374 \pm 881$	$1603 \pm 468 \pm 180 \pm 326$
2P WP	$6809 \pm 1986 \pm 700 \pm 1077$	$2399 \pm 700 \pm 264 \pm 393$	$1209 \pm 353 \pm 136 \pm 129$
3P OP		$7586 \pm 1529 \pm 784 \pm 2690$	$2290 \pm 462 \pm 251 \pm 638$
3P WP		$4831 \pm 974 \pm 486 \pm 1313$	$1597 \pm 322 \pm 173 \pm 292$
$\sqrt{s}(\text{GeV})$	5.00	10.6	11.2
1P OP	$568 \pm 154 \pm 55 \pm 5 \pm 34$	$15.0 \pm 4.1 \pm 0.8 \pm 2.1 \pm 2.8$	$11.9 \pm 3.2 \pm 0.6 \pm 1.8 \pm 2.3$
1P WP	$505 \pm 137 \pm 49 \pm 26 \pm 40$	$14.7 \pm 4.0 \pm 0.8 \pm 2.3 \pm 2.7$	$11.7 \pm 3.2 \pm 0.6 \pm 1.9 \pm 2.3$
2P OP	$915 \pm 267 \pm 102 \pm 145$	$10.4 \pm 3.0 \pm 0.7 \pm 1.2$	$8.2 \pm 2.4 \pm 0.5 \pm 1.0$
2P WP	$720 \pm 210 \pm 81 \pm 47$	$10.0 \pm 2.9 \pm 0.7 \pm 1.4$	$7.9 \pm 2.3 \pm 0.5 \pm 1.1$
3P OP	$1061 \pm 214 \pm 119 \pm 234$	$7.6 \pm 1.5 \pm 0.5 \pm 0.8$	$5.9 \pm 1.2 \pm 0.4 \pm 0.6$
3P WP	$786 \pm 159 \pm 88 \pm 97$	$7.3 \pm 1.5 \pm 0.5 \pm 0.9$	$5.7 \pm 1.1 \pm 0.4 \pm 0.8$

Unfortunately, they obtain significantly different cross sections for the production of these near-threshold particles for the excited P -wave states. We remain the strategy in our previous work to set the quark mass to the half of the meson. The results are shown in Tab.5, 6, 7 8 and in Fig.9, 10, 11, 12. The numerical cross sections for $\eta_c(2S)$ states positively increase compared with those for $\mathcal{O}(\alpha_s + v^2)$. Meanwhile, the cross-sections for the excited P -wave states are lower than those from the previous $\mathcal{O}(\alpha_s + v^2)$ results. However for $\eta_c(3S)$ state, the numerical values are still assigned to BESIII to determine the states. For excited P -wave states, the cross sections come down compared with the previous $\mathcal{O}(\alpha_s + v^2)$ results. But the numerical values are still referred for BESIII to find these states.

As discussed in our previous works, the results of $\eta_c(mS)$ and $\chi_{cJ}(nP)$ states are helpful charify the nature of XYZ particles with the even charge conjugation, such as $X(3872)$, $X(3940)$, $X(4160)$ and $X(4350)$. Taking $X(3872)$ state for an example, we considered it as the mixture with $\chi_{c1}(2P)$ component[72], therefore, the cross sections for $X(3872)$ are determined by

$$d\sigma[e^+e^- \rightarrow \gamma X(3872) \rightarrow \gamma J/\psi \pi^+ \pi^-] = d\sigma[e^+e^- \rightarrow \gamma \chi_{c1}(2P)] \times k, \quad (4.7)$$

where $k = Z_{c\bar{c}}^{X(3872)} \times Br[X(3872) \rightarrow J/\psi \pi^+ \pi^-]$. $Br[X(3872) \rightarrow J/\psi \pi^+ \pi^-]$ is the branching fraction for $X(3872)$ decay to $J/\psi \pi^+ \pi^-$. $Z_{c\bar{c}}^{X(3872)}$ is the probability of the $\chi_{c1}(2P)$ component in $X(3872)$. $k = 0.018 \pm 0.04$ [49, 78]. With the results up-to $\mathcal{O}(\alpha_s v^2)$, we revisit the cross sections for $X(3872)$ shown in Fig.13. In the figure, we also give the total cross sections at

Table 8. The total cross sections in fb up to $\alpha_s v^2$ order of $e^+e^- \rightarrow \chi_{c2}(nP) + \gamma$ with $n = 1, 2, 3$ in the BESIII and B-factories energy region. WP and OP indicate considering or ignoring the phase space contributions, respectively. The uncertainties in each cell come from the uncertainties of the wave functions at the origin, α_s , $\langle v^2 \rangle$, and charm quark mass m_c in turns. For the excited states, we select the charm quark mass as the half of the meson mass in the calculations, therefore there are no m_c uncertainties. The mass of $\chi_{c2}(nP)$ is selected as 3.927GeV and 4.208GeV for $n = 2, 3$ respectively[74, 80].

$\sqrt{s}(\text{GeV})$	4.25	4.50	4.75
1P OP	$1375 \pm 374 \pm 211 \pm 192 \pm 267$	$799 \pm 217 \pm 128 \pm 92 \pm 112$	$497 \pm 135 \pm 82 \pm 47 \pm 50$
1P WP	$1178 \pm 320 \pm 179 \pm 94 \pm 193$	$701 \pm 191 \pm 111 \pm 43 \pm 82$	$443 \pm 121 \pm 73 \pm 21 \pm 36$
2P OP	$17037 \pm 4969 \pm 1898 \pm 6041$	$4564 \pm 1331 \pm 568 \pm 1305$	$1878 \pm 548 \pm 252 \pm 444$
2P WP	$11250 \pm 3281 \pm 1205 \pm 3147$	$3316 \pm 967 \pm 402 \pm 681$	$1451 \pm 423 \pm 190 \pm 230$
3P OP		$13164 \pm 2654 \pm 1424 \pm 4895$	$3253 \pm 656 \pm 395 \pm 983$
3P WP		$8465 \pm 1707 \pm 878 \pm 2546$	$2314 \pm 466 \pm 273 \pm 513$
$\sqrt{s}(\text{GeV})$	5.00	10.6	11.2
1P OP	$325 \pm 88 \pm 55 \pm 25 \pm 23$	$3.1 \pm 0.8 \pm 0.8 \pm 0.2 \pm 0.4$	$2.3 \pm 0.6 \pm 0.6 \pm 0.2 \pm 0.3$
1P WP	$294 \pm 80 \pm 50 \pm 10 \pm 16$	$3.0 \pm 0.8 \pm 0.8 \pm 0.2 \pm 0.4$	$2.3 \pm 0.6 \pm 0.6 \pm 0.2 \pm 0.3$
2P OP	$945 \pm 275 \pm 133 \pm 188$	$2.7 \pm 0.8 \pm 0.6 \pm 0.1$	$2.0 \pm 0.6 \pm 0.5 \pm 0.1$
2P WP	$761 \pm 222 \pm 106 \pm 96$	$2.6 \pm 0.8 \pm 0.6 \pm 0.1$	$1.9 \pm 0.6 \pm 0.5 \pm 0.1$
3P OP	$1305 \pm 263 \pm 171 \pm 328$	$2.2 \pm 0.4 \pm 0.5 \pm 0.$	$1.6 \pm 0.3 \pm 0.4 \pm 0.$
3P WP	$990 \pm 200 \pm 127 \pm 171$	$2.1 \pm 0.4 \pm 0.5 \pm 0.1$	$1.5 \pm 0.3 \pm 0.3 \pm 0.1$

the data points for the BESIII measurements including the contributions from the resonances ($\psi(4040)$ and $\psi(4160)$) which have been discussed in our previous paper and are listed here

$$\begin{aligned}
&(\sigma_{\psi(4040)}[4.23] + \sigma_{\psi(4160)}[4.23]) \times k = (62 \pm 14)fb, \\
&(\sigma_{\psi(4040)}[4.26] + \sigma_{\psi(4160)}[4.26]) \times k = (37 \pm 8)fb.
\end{aligned} \tag{4.8}$$

From the figure, the cross sections for the predictions of $X(3872)$ may be smaller than the experiment data, but one still can not jump to conclusions for the nature of the $X(3872)$ and the more data are required.

5 Summary

In this study, we extend our previous works on the production of charmonia with even charge conjugation in the processes $e^+e^- \rightarrow \eta_c(nS)(\chi_{cJ}(mP)) + \gamma$ up to the $\mathcal{O}(\alpha_s v^2)$ corrections. The results indicate that these corrections exhibit a logarithmic singularity of $\ln(1-r)$, which is not observed in the $\mathcal{O}(\alpha_s)$ corrections near the threshold. The $\mathcal{O}(\alpha_s v^2)$ corrections also contribute to the total cross-sections near the threshold and are important to the diphoton decay for the χ_{c0} and χ_{c2} states. We revisit the numerical calculations to the cross-sections for the $\eta_c(nS)$ and $\chi_{cJ}(mP)$ states using the results for the $\mathcal{O}(\alpha_s v^2)$ corrections.

Acknowledgments

The authors would like to thank Professor C.P. Shen for useful discussion. This work was supported by the National Natural Science Foundation of China (Grants No. 11375021), the Foundation for the Author of National Excellent Doctoral Dissertation of China (Grants No. 2007B18 and No. 201020), the New Century Excellent Talents in University (NCET) under grant NCET-13-0030, the Major State Basic Research Development Program of China (No. 2015CB856701), and the Education Ministry of LiaoNing Province.

6 Appendix

In this section, we give the matching results of the short-distance coefficients for η_c process. The Lorentz invariance determines the amplitude should have the form of

$$A\epsilon^{\mu\nu\rho\tau}(\epsilon_Q^*)_\mu(\epsilon_k^*)_\nu k_\rho p_\tau.$$

Therefore the coefficients in $v^{(0)}$ must be like $A^{(0)}\epsilon_1$. The $\mathcal{O}(v^2)$ coefficients obtained in proceed of derivate the amplitude will be like $A^{(v^2)}\epsilon_1 + B^{(v^2)}\epsilon_2$. ϵ_1 and ϵ_2 have defined as Eq.(2.25). Therefore we write the $\mathcal{O}(v^2)$ short-distance coefficients into a plus of three parts as seen in the following results. The third term is just to cancel the $\mathcal{O}(v^2)$ contributions from the relativistic normalization factor in Eq.(2.12). And we omit the imaginary parts in the coefficients in $\mathcal{O}(\alpha_s)$ and $\mathcal{O}(\alpha_s v^2)$, which do't contribute to cross sections at order of $\mathcal{O}(\alpha_s v^2)$.

$$d^{(0)} \equiv A^{(0)}\epsilon_1 = \frac{(4\pi\alpha)Q_c^2 r}{2m_c^3(1-r)}\epsilon_1. \quad (6.1)$$

$$d^{(v^2)} = -\frac{(4\pi\alpha)Q_c^2 r(5-17r)}{24m_c^5(1-r)^2}\epsilon_1 + \frac{A^{(0)}}{m_c^2}\epsilon_2 - \frac{d^{(0)}}{4m_c^2}. \quad (6.2)$$

$$\begin{aligned} d^{(\alpha_s)} \equiv A^{(\alpha_s)}\epsilon_1 &= \frac{(4\pi\alpha)(4\pi\alpha_s)Q_c^2 C_A C_F r}{96\pi^2 m_c^3 N_c (2-r)^2 (1-r)^2} \epsilon_1 \\ &\{ -6(1-r)[5r^2 - r(19 + \ln 16) + 18 + \ln 64] - \pi^2(1+r)(2-r)^2 + 6[r(r+2) - 6] \ln r \\ &+ 18(2-r)^2[(1 - \sqrt{1-r}) \ln(1 - \sqrt{1-r}) + (1 + \sqrt{1-r}) \ln(1 + \sqrt{1-r})] \\ &- 12(1-r)(3-2r) \ln(1-r) + 3(2-r)^2[r \text{Li}_2(\frac{2}{r} - 1) + (2+r)(\text{Li}_2(\frac{2}{1 - \sqrt{1-r}}) \\ &+ \text{Li}_2(\frac{2}{1 + \sqrt{1-r}}) + \text{Li}_2(\frac{r}{2-r}) - \text{Li}_2(\frac{2}{2-r}) - \text{Li}_2(\frac{2}{r})) \}. \end{aligned} \quad (6.3)$$

$$\begin{aligned}
d^{(\alpha_s v^2)} = & -\frac{(4\pi\alpha)(4\pi\alpha_s)Q_c^2 C_A C_F r}{1152\pi^2 m_c^5 N_c (2-r)^4 (1-r)^3} \epsilon_1 \\
& \{ -2(1-r)[r^5(96\ln 2 - 211) - 156r^4(3\ln 2 - 10) + 23r^3(30\ln 2 - 181) \\
& + r^2(4598 - 606\ln 2) + 36r(24\ln 2 - 37) - 8(79 + 87\ln 2)] + \pi^2(21r^2 + 28r - 5)(2-r)^4 \\
& - 6(32r^6 - 251r^5 + 889r^4 - 1936r^3 + 2482r^2 - 1496r + 216)\ln r \\
& - 6(2-r)^4(63r+1)[(1-\sqrt{1-r})\ln(1-\sqrt{1-r}) + (1+\sqrt{1-r})\ln(1+\sqrt{1-r})] \\
& - 12(1-r)(16r^5 - 78r^4 + 115r^3 - 101r^2 + 144r - 116)\ln(1-r) \\
& - 3(2-r)^4[3r(1+7r)\text{Li}_2(\frac{2}{r}-1) + (21r^2 + 53r - 10)(\text{Li}_2(\frac{2}{1-\sqrt{1-r}}) \\
& + \text{Li}_2(\frac{2}{1+\sqrt{1-r}}) + \text{Li}_2(\frac{r}{2-r}) - \text{Li}_2(\frac{2}{2-r}) - \text{Li}_2(\frac{2}{r}))] \} + \frac{A^{(\alpha_s)}}{m_c^2} \epsilon_2 - \frac{d^{(\alpha_s)}}{4m_c^2}. \tag{6.4}
\end{aligned}$$

References

- [1] G. T. Bodwin, E. Braaten, and G. P. Lepage, *Rigorous QCD analysis of inclusive annihilation and production of heavy quarkonium*, *Phys.Rev.* **D51** (1995) 1125–1171, [[hep-ph/9407339](#)].
- [2] N. Brambilla, E. Mereghetti, and A. Vairo, *Hadronic quarkonium decays at order v^7* , *Phys.Rev.* **D79** (2009) 074002, [[arXiv:0810.2259](#)].
- [3] J. Lansberg and T. Pham, *Effective Lagrangian for Two-photon and Two-gluon Decays of P-wave Heavy Quarkonium $\chi_{c0,2}$ and $\chi_{b0,2}$ states*, *Phys.Rev.* **D79** (2009) 094016, [[arXiv:0903.1562](#)].
- [4] Z.-G. He, Y. Fan, and K.-T. Chao, *QCD prediction for the non- $D\bar{D}$ annihilation decay of $\psi(3770)$* , *Phys. Rev. Lett.* **101** (2008) 112001, [[arXiv:0802.1849](#)].
- [5] Z.-G. He, Y. Fan, and K.-T. Chao, *NRQCD Predictions of D-Wave Quarkonia $^3D_J (J=1,2,3)$ Decay into Light Hadrons at Order α_s^3* , *Phys.Rev.* **D81** (2010) 074032, [[arXiv:0910.3939](#)].
- [6] Y. Fan, Z.-G. He, Y.-Q. Ma, and K.-T. Chao, *Predictions of Light Hadronic Decays of Heavy Quarkonium 1D_2 States in NRQCD*, *Phys. Rev.* **D80** (2009) 014001, [[arXiv:0903.4572](#)].
- [7] **Belle** Collaboration, K. Abe et al., *Observation of double $c\bar{c}$ production in e^+e^- annihilation at \sqrt{s} approx. 10.6-GeV*, *Phys. Rev. Lett.* **89** (2002) 142001, [[hep-ex/0205104](#)].
- [8] **BABAR** Collaboration, B. Aubert et al., *Measurement of double charmonium production in e^+e^- annihilations at $\sqrt{s} = 10.6$ GeV*, *Phys. Rev.* **D72** (2005) 031101, [[hep-ex/0506062](#)].
- [9] K.-Y. Liu, Z.-G. He, and K.-T. Chao, *Problems of double charm production in e^+e^- annihilation at $\sqrt{s} = 10.6$ GeV.*, *Phys. Lett.* **B557** (2003) 45–54, [[hep-ph/0211181](#)].
- [10] E. Braaten and J. Lee, *Exclusive double-charmonium production in e^+e^- annihilation*, *Phys. Rev.* **D67** (2003) 054007, [[hep-ph/0211085](#)].
- [11] K.-Y. Liu, Z.-G. He, and K.-T. Chao, *Inclusive charmonium production via double $c\bar{c}$ in e^+e^- annihilation*, *Phys. Rev.* **D69** (2004) 094027, [[hep-ph/0301218](#)].
- [12] K.-Y. Liu, Z.-G. He, and K.-T. Chao, *Production of $J/\psi + c\bar{c}$ through two photons in e^+e^- annihilation*, *Phys. Rev.* **D68** (2003) 031501, [[hep-ph/0305084](#)].

- [13] K.-Y. Liu, Z.-G. He, and K.-T. Chao, *Search for excited charmonium states in e^+e^- annihilation at $\sqrt{s} = 10.6\text{-GeV}$* , *Phys.Rev.* **D77** (2008) 014002, [[hep-ph/0408141](#)].
- [14] K.-Y. Liu and K.-T. Chao, *S-D mixing and $\psi(3770)$ production in e^+e^- annihilation and B decay and its radiative transitions*, *Phys.Rev.* **D70** (2004) 094001, [[hep-ph/0405126](#)].
- [15] Y.-J. Zhang, Y.-J. Gao, and K.-T. Chao, *Next-to-leading order QCD correction to $e^+e^- \rightarrow J/\psi\eta_c$ at $\sqrt{s} = 10.6\text{ GeV}$* , *Phys.Rev.Lett.* **96** (2006) 092001, [[hep-ph/0506076](#)].
- [16] Y.-J. Zhang and K.-T. Chao, *Double charm production $e^+e^- \rightarrow J/\psi + c\bar{c}$ at B factories with next-to-leading order QCD correction*, *Phys.Rev.Lett.* **98** (2007) 092003, [[hep-ph/0611086](#)].
- [17] K. Wang, Y.-Q. Ma, and K.-T. Chao, *QCD corrections to $e^+e^- \rightarrow J/\psi(\psi(2S)) + \chi_{cJ}(J = 0, 1, 2)$ at B Factories*, *Phys.Rev.* **D84** (2011) 034022, [[arXiv:1107.2646](#)].
- [18] Y.-J. Zhang, Y.-Q. Ma, and K.-T. Chao, *Factorization and NLO QCD correction in $e^+e^- \rightarrow J/\psi(\psi(2S)) + \chi_{c0}$ at B Factories*, *Phys. Rev.* **D78** (2008) 054006, [[arXiv:0802.3655](#)].
- [19] Y.-J. Zhang, Y.-Q. Ma, K. Wang, and K.-T. Chao, *QCD radiative correction to color-octet J/ψ inclusive production at B Factories*, *Phys.Rev.* **D81** (2010) 034015, [[arXiv:0911.2166](#)].
- [20] B. Gong and J.-X. Wang, *QCD corrections to J/ψ plus η_c production in e^+e^- annihilation at $\sqrt{s} = 10.6\text{-GeV}$* , *Phys. Rev.* **D77** (2008) 054028, [[arXiv:0712.4220](#)].
- [21] B. Gong and J.-X. Wang, *QCD corrections to double J/ψ production in e^+e^- annihilation at $\sqrt{s} = 10.6\text{-GeV}$* , *Phys. Rev. Lett.* **100** (2008) 181803, [[arXiv:0801.0648](#)].
- [22] B. Gong and J.-X. Wang, *Next-to-Leading-Order QCD Corrections to $e^+e^- \rightarrow J/\psi c\bar{c}$ at the B Factories*, [arXiv:0904.1103](#).
- [23] B. Gong and J.-X. Wang, *Next-to-Leading-Order QCD Corrections to $e^+e^- \rightarrow J/\psi + gg$ at the B Factories*, *Phys. Rev. Lett.* **102** (2009) 162003, [[arXiv:0901.0117](#)].
- [24] Y.-Q. Ma, Y.-J. Zhang, and K.-T. Chao, *QCD correction to $e^+e^- \rightarrow J/\psi gg$ at B Factories*, *Phys. Rev. Lett.* **102** (2009) 162002, [[arXiv:0812.5106](#)].
- [25] H.-R. Dong, F. Feng, and Y. Jia, *$O(\alpha_s)$ corrections to $J/\psi + \chi_{cJ}$ production at B factories*, *JHEP* **1110** (2011) 141, [[arXiv:1107.4351](#)].
- [26] G. T. Bodwin, H. S. Chung, and J. Lee, *Double Logarithms in $e^+e^- \rightarrow J/\psi + \eta_c$* , [arXiv:1406.1926](#).
- [27] Z.-G. He, Y. Fan, and K.-T. Chao, *Relativistic corrections to J/ψ exclusive and inclusive double charm production at B factories*, *Phys.Rev.* **D75** (2007) 074011, [[hep-ph/0702239](#)].
- [28] G. T. Bodwin, D. Kang, T. Kim, J. Lee, and C. Yu, *Relativistic corrections to $e^+e^- \rightarrow J/\psi + \eta_c$ in a potential model*, [hep-ph/0611002](#).
- [29] D. Ebert and A. P. Martynenko, *Relativistic effects in the production of pseudoscalar and vector doubly heavy mesons from e^+e^- annihilation*, *Phys. Rev.* **D74** (2006) 054008, [[hep-ph/0605230](#)].
- [30] G. T. Bodwin, J. Lee, and C. Yu, *Resummation of Relativistic Corrections to $e^+e^- \rightarrow J/\psi + \eta_c$* , *Phys.Rev.* **D77** (2008) 094018, [[arXiv:0710.0995](#)].

- [31] E. Elekina and A. Martynenko, *Relativistic effects in the double S- and P-wave charmonium production in e^+e^- annihilation*, *Phys.Rev.* **D81** (2010) 054006, [[arXiv:0910.0394](#)].
- [32] Y. Jia, *Color-singlet relativistic correction to inclusive J/ψ production associated with light hadrons at B factories*, *Phys.Rev.* **D82** (2010) 034017, [[arXiv:0912.5498](#)].
- [33] Z.-G. He, Y. Fan, and K.-T. Chao, *Relativistic correction to $e^+e^- \rightarrow J/\psi + gg$ at B factories and constraint on color-octet matrix elements*, *Phys.Rev.* **D81** (2010) 054036, [[arXiv:0910.3636](#)].
- [34] Y. Fan, J. Lee, and C. Yu, *Resummation of relativistic corrections to exclusive productions of charmonia in e^+e^- collisions*, [arXiv:1211.4111](#).
- [35] Y. Fan, J. Lee, and C. Yu, *Higher-order corrections to exclusive production of charmonia at B factories*, [arXiv:1209.1875](#).
- [36] H.-R. Dong, F. Feng, and Y. Jia, *$O(\alpha_s v^2)$ correction to $e^+e^- \rightarrow J/\psi + \eta_c$ at B factories*, *Phys.Rev.* **D85** (2012) 114018, [[arXiv:1204.4128](#)].
- [37] X.-H. Li and J.-X. Wang, *$O(\alpha_s v^2)$ correction to J/ψ plus η_c production in e^+e^- annihilation at $\sqrt{s}=10.6\text{GeV}$* , [arXiv:1301.0376](#).
- [38] J. M. Campbell, F. Maltoni, and F. Tramontano, *QCD corrections to J/ψ and Υ production at hadron colliders*, *Phys.Rev.Lett.* **98** (2007) 252002, [[hep-ph/0703113](#)].
- [39] B. Gong and J.-X. Wang, *QCD corrections to polarization of J/ψ and Υ at Tevatron and LHC*, *Phys. Rev.* **D78** (2008) 074011, [[arXiv:0805.2469](#)].
- [40] B. Gong and J.-X. Wang, *Next-to-leading-order QCD corrections to J/ψ polarization at Tevatron and Large-Hadron-Collider energies*, *Phys. Rev. Lett.* **100** (2008) 232001, [[arXiv:0802.3727](#)].
- [41] L. Gang, W. ShuangTe, S. Mao, and L. JiPing, *Prompt heavy quarkonium production in association with a massive (anti)bottom quark at the LHC*, *Phys.Rev.* **D85** (2012) 074026, [[arXiv:1203.0799](#)].
- [42] Y.-Q. Ma, K. Wang, and K.-T. Chao, *$J/\psi(\psi')$ production at the Tevatron and LHC at $O(\alpha_s^4 v^4)$ in nonrelativistic QCD*, *Phys.Rev.Lett.* **106** (2011) 042002, [[arXiv:1009.3655](#)].
- [43] Y.-Q. Ma, K. Wang, and K.-T. Chao, *QCD radiative corrections to χ_{cJ} production at hadron colliders*, *Phys.Rev.* **D83** (2011) 111503, [[arXiv:1002.3987](#)].
- [44] Y.-Q. Ma, K. Wang, and K.-T. Chao, *A complete NLO calculation of the J/ψ and ψ' production at hadron colliders*, *Phys.Rev.* **D84** (2011) 114001, [[arXiv:1012.1030](#)].
- [45] H.-S. Shao, *HELAC-Onia: an automatic matrix element generator for heavy quarkonium physics*, [arXiv:1212.5293](#).
- [46] M. Butenschoen and B. A. Kniehl, *Reconciling J/ψ production at HERA, RHIC, Tevatron, and LHC with NRQCD factorization at next-to-leading order*, *Phys.Rev.Lett.* **106** (2011) 022003, [[arXiv:1009.5662](#)].
- [47] K. Wang, Y.-Q. Ma, and K.-T. Chao, *$\Upsilon(1S)$ prompt production at the Tevatron and LHC in nonrelativistic QCD*, *Phys.Rev.* **D85** (2012) 114003, [[arXiv:1202.6012](#)].
- [48] M. Butenschoen, Z.-G. He, and B. A. Kniehl, *NLO NRQCD disfavors the interpretation of $X(3872)$ as $\chi_{c1}(2P)$* , [arXiv:1303.6524](#).

- [49] C. Meng, H. Han, and K.-T. Chao, *X(3872) and its production at hadron colliders*, [arXiv:1304.6710](#).
- [50] R. Li and J.-X. Wang, *Next-to-Leading-Order study on the associate production of $J/\psi + \gamma$ at the LHC*, *Phys.Rev.* **D89** (2014) 114018, [[arXiv:1401.6918](#)].
- [51] J.-X. Wang and H.-F. Zhang, *h_c Production at Hadron Colliders*, [arXiv:1403.5944](#).
- [52] L.-P. Sun, H. Han, and K.-T. Chao, *Impact of J/ψ pair production at the LHC and predictions in nonrelativistic QCD*, [arXiv:1404.4042](#).
- [53] G. T. Bodwin, H. S. Chung, U.-R. Kim, and J. Lee, *Fragmentation contributions to J/ψ production at the Tevatron and the LHC*, *Phys.Rev.Lett.* **113** (2014) 022001, [[arXiv:1403.3612](#)].
- [54] K.-T. Chao, Y.-Q. Ma, H.-S. Shao, K. Wang, and Y.-J. Zhang, *J/ψ polarization at hadron colliders in nonrelativistic QCD*, *Phys.Rev.Lett.* **108** (2012) 242004, [[arXiv:1201.2675](#)].
- [55] M. Butenschoen and B. A. Kniehl, *J/ψ polarization at Tevatron and LHC: Nonrelativistic-QCD factorization at the crossroads*, *Phys.Rev.Lett.* **108** (2012) 172002, [[arXiv:1201.1872](#)].
- [56] B. Gong, L.-P. Wan, J.-X. Wang, and H.-F. Zhang, *Polarization for Prompt $J/\psi, \psi(2s)$ production at the Tevatron and LHC*, *Phys.Rev.Lett.* **110** (2013) 042002, [[arXiv:1205.6682](#)].
- [57] B. Gong, L.-P. Wan, J.-X. Wang, and H.-F. Zhang, *Complete next-to-leading-order study on the yield and polarization of $\Upsilon(1S, 2S, 3S)$ at the Tevatron and LHC*, [arXiv:1305.0748](#).
- [58] H.-S. Shao and K.-T. Chao, *Spin correlations in polarizations of P-wave charmonia χ_{cJ} and impact on J/ψ polarization*, [arXiv:1209.4610](#).
- [59] H.-S. Shao, Y.-Q. Ma, K. Wang, and K.-T. Chao, *Polarizations of χ_{c1} and χ_{c2} in prompt production at the LHC*, *Phys.Rev.Lett.* **112** (2014) 182003, [[arXiv:1402.2913](#)].
- [60] Y. Fan, Y.-Q. Ma, and K.-T. Chao, *Relativistic Correction to J/ψ Production at Hadron Colliders*, *Phys. Rev.* **D79** (2009) 114009, [[arXiv:0904.4025](#)].
- [61] G.-Z. Xu, Y.-J. Li, K.-Y. Liu, and Y.-J. Zhang, *Relativistic Correction to Color Octet J/ψ Production at Hadron Colliders*, *Phys.Rev.* **D86** (2012) 094017, [[arXiv:1203.0207](#)].
- [62] Y.-J. Li, G.-Z. Xu, K.-Y. Liu, and Y.-J. Zhang, *Relativistic Correction to J/ψ and Υ Pair Production*, [arXiv:1303.1383](#).
- [63] Y. Jia, X.-T. Yang, W.-L. Sang, and J. Xu, *$O(\alpha_s v^2)$ correction to pseudoscalar quarkonium decay to two photons*, *JHEP* **1106** (2011) 097, [[arXiv:1104.1418](#)].
- [64] H.-K. Guo, Y.-Q. Ma, and K.-T. Chao, *$O(\alpha_s v^2)$ Corrections to Hadronic and Electromagnetic Decays of 1S_0 Heavy Quarkonium*, *Phys. Rev.* **D83** (2011) 114038, [[arXiv:1104.3138](#)].
- [65] J.-Z. Li, Y.-Q. Ma, and K.-T. Chao, *QCD and Relativistic $O(\alpha_s v^2)$ Corrections to Hadronic Decays of Spin-Singlet Heavy Quarkonia h_c, h_b and η_b* , [arXiv:1209.4011](#).
- [66] N. Brambilla, S. Eidelman, B. Heltsley, R. Vogt, G. Bodwin, et al., *Heavy quarkonium: progress, puzzles, and opportunities*, *Eur.Phys.J.* **C71** (2011) 1534, [[arXiv:1010.5827](#)].
- [67] H. S. Chung, J. Lee, and C. Yu, *Exclusive heavy quarkonium $+ \gamma$ production from e^+e^- annihilation into a virtual photon*, *Phys.Rev.* **D78** (2008) 074022, [[arXiv:0808.1625](#)].

- [68] V. Braguta, *Exclusive $C=+$ charmonium production in $e^+e^- \rightarrow H + \gamma$ at B-factories within light cone formalism*, *Phys.Rev.* **D82** (2010) 074009, [[arXiv:1006.5798](#)].
- [69] D. Li, Z.-G. He, and K.-T. Chao, *Search for $C=+$ charmonium and bottomonium states in $e^+e^- \rightarrow \gamma + X$ at B factories*, *Phys.Rev.* **D80** (2009) 114014, [[arXiv:0910.4155](#)].
- [70] W.-L. Sang and Y.-Q. Chen, *Higher Order Corrections to the Cross Section of $e^+e^- \rightarrow \text{Quarkonium} + \gamma$* , *Phys.Rev.* **D81** (2010) 034028, [[arXiv:0910.4071](#)].
- [71] W.-L. Sang, Y.-J. Gao, and Y.-Q. Chen, *Indirect measurement of quarkonium in the two-photon process*, *Phys.Rev.* **D86** (2012) 074031.
- [72] Y.-J. Li, G.-Z. Xu, K.-Y. Liu, and Y.-J. Zhang, *Search for $C = +$ charmonium and XYZ states in $e^+e^- \rightarrow \gamma + H$ at BESIII*, *JHEP* **1401** (2014) 022, [[arXiv:1310.0374](#)].
- [73] K.-T. Chao, Z.-G. He, D. Li, and C. Meng, *Search for $C = +$ charmonium states in $e^+e^- \rightarrow \gamma + X$ at BEPCII/BESIII*, [arXiv:1310.8597](#).
- [74] B.-Q. Li and K.-T. Chao, *Higher Charmonia and X,Y,Z states with Screened Potential*, *Phys.Rev.* **D79** (2009) 094004, [[arXiv:0903.5506](#)].
- [75] R. Molina and E. Oset, *The $Y(3940)$, $Z(3930)$ and the $X(4160)$ as dynamically generated resonances from the vector-vector interaction*, *Phys.Rev.* **D80** (2009) 114013, [[arXiv:0907.3043](#)].
- [76] B.-Q. Li, C. Meng, and K.-T. Chao, *Search for $\chi_{cJ}(2P)$ from Higher Charmonium $E1$ Transitions and X,Y,Z States*, [arXiv:1201.4155](#).
- [77] **Belle Collaboration** Collaboration, S. Choi et al., *Observation of a narrow charmonium - like state in exclusive $B^{+-} \rightarrow K^{+-}\pi^+\pi^- J/\psi$ decays*, *Phys.Rev.Lett.* **91** (2003) 262001, [[hep-ex/0309032](#)].
- [78] C. Meng, Y.-J. Gao, and K.-T. Chao, *$B \rightarrow \chi_{c1}(1P, 2P)K$ decays in QCD factorization and $X(3872)$* , [hep-ph/0506222](#).
- [79] **BESIII Collaboration** Collaboration, M. Ablikim et al., *Observation of $e^+e^- \rightarrow \gamma X(3872)$ at BESIII*, *Phys.Rev.Lett.* **112** (2014) 092001, [[arXiv:1310.4101](#)].
- [80] **Particle Data Group** Collaboration, J. Beringer et al., *Review of Particle Physics (RPP)*, *Phys.Rev.* **D86** (2012) 010001.
- [81] F.-K. Guo and U.-G. Meissner, *Where is the $\chi_{c0}(2P)$?*, *Phys.Rev.* **D86** (2012) 091501, [[arXiv:1208.1134](#)].
- [82] G. T. Bodwin and A. Petrelli, *Order v^4 corrections to S-wave quarkonium decay*, *Phys. Rev.* **D66** (2002) 094011, [[hep-ph/0205210](#)].
- [83] A. Denner and S. Dittmaier, *Reduction schemes for one-loop tensor integrals*, *Nucl. Phys.* **B734** (2006) 62–115, [[hep-ph/0509141](#)].
- [84] T. Hahn, *Generating feynman diagrams and amplitudes with FeynArts 3*, *Comput. Phys. Commun.* **140** (2001) 418–431, [[hep-ph/0012260](#)].
- [85] T. Hahn and M. Perez-Victoria, *Automatized one-loop calculations in four and D dimensions*, *Comput. Phys. Commun.* **118** (1999) 153–165, [[hep-ph/9807565](#)].

- [86] R. Mertig, M. Bohm, and A. Denner, *FEYNALC: Computer algebraic calculation of feynman amplitudes*, *Comput. Phys. Commun.* **64** (1991) 345–359.
- [87] J. Ma and Q. Wang, *Corrections for two photon decays of $\chi(c0)$ and $\chi(c2)$ and color octet contributions*, *Phys.Lett.* **B537** (2002) 233–240, [[hep-ph/0203082](#)].
- [88] E. J. Eichten and C. Quigg, *Quarkonium wave functions at the origin*, *Phys. Rev.* **D52** (1995) 1726–1728, [[hep-ph/9503356](#)].
- [89] M. Beneke, I.Z. Rothstein, and Mark B. Wise. Kinematic enhancement of nonperturbative corrections to quarkonium production. *Phys.Lett.*, B408:373–380, 1997.
- [90] M. Beneke, G. A. Schuler, and S. Wolf. Quarkonium momentum distributions in photoproduction and B decay. *Phys. Rev.*, D62:034004, 2000.
- [91] Dirk Kreimer. The Role of $\gamma(5)$ in dimensional regularization. 1993.
- [92] S.A. Larin. The Renormalization of the axial anomaly in dimensional regularization. *Phys.Lett.*, B303:113–118, 1993.
- [93] Gerard 't Hooft and M. J. G. Veltman. Scalar one loop integrals. *Nucl. Phys.*, B153:365–401, 1979.
- [94] Gerard 't Hooft and M.J.G. Veltman. Regularization and Renormalization of Gauge Fields. *Nucl.Phys.*, B44:189–213, 1972.
- [95] P. Breitenlohner and D. Maison. Dimensional Renormalization and the Action Principle. *Commun.Math.Phys.*, 52:11–38, 1977.
- [96] Todd H. West. FeynmanParameter and Trace: Programs for expressing Feynman amplitudes as integrals over Feynman parameters. *Comput.Phys.Comm.*, 77:286–298, 1993.
- [97] S.A. Larin and J.A.M. Vermaseren. The α_s^3 corrections to the Bjorken sum rule for polarized electroproduction and to the Gross-Llewellyn Smith sum rule. *Phys.Lett.*, B259:345–352, 1991.
- [98] J.G. Korner, D. Kreimer, and K. Schilcher. A Practicable $\gamma(5)$ scheme in dimensional regularization. *Z.Phys.*, C54:503–512, 1992.
- [99] Gerard 't Hooft. Symmetry Breaking Through Bell-Jackiw Anomalies. *Phys.Rev.Lett.*, 37:8–11, 1976.

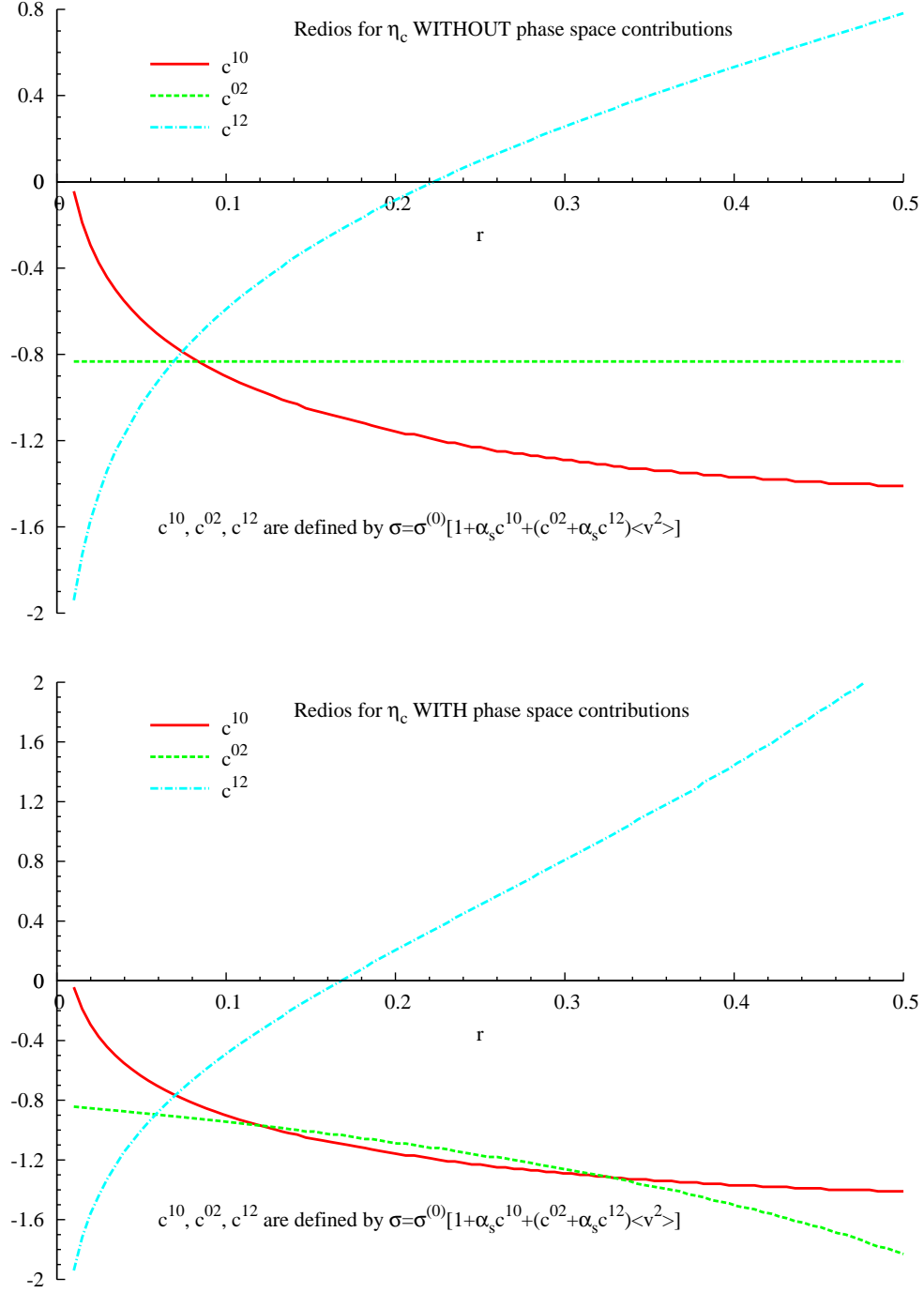


Figure 2. The relative ratios for the corrections in the order of α_s , v^2 , and $\alpha_s v^2$ to the LO cross section for η_c production recoiled with a hard photon as a function of r . The ratios c^{10} , c^{02} , and c^{11} are defined by the expression $\sigma = \hat{\sigma}^{(0)} [1 + \alpha_s c^{10} + (c^{02} + \alpha_s c^{12}) \langle v^2 \rangle] \langle 0 | \mathcal{O}^H | 0 \rangle$.

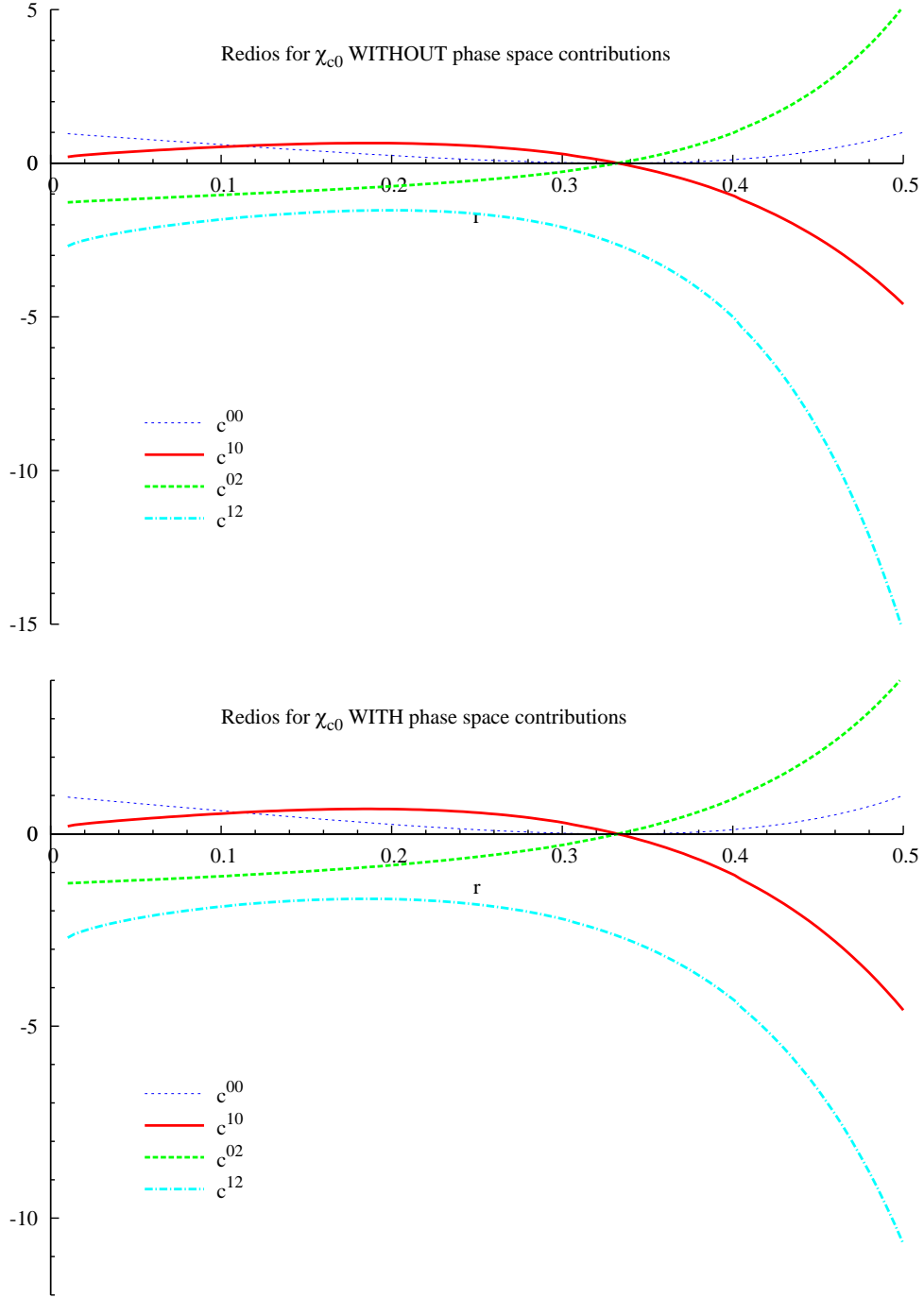


Figure 3. The relative ratios for the corrections in the order of α_s , v^2 , and $\alpha_s v^2$ to the LO cross section for χ_{c0} production recoiled with a hard photon as a function of r . The ratios c^{10} , c^{02} , and c^{11} are defined by the expression $\sigma = \frac{(4\pi\alpha)^3 Q_c^4}{18\pi m_c^3 s^2} [c^{00} + \alpha_s c^{10} + (c^{02} + \alpha_s c^{12}) \langle v^2 \rangle] \langle 0 | \mathcal{O}^H | 0 \rangle$.

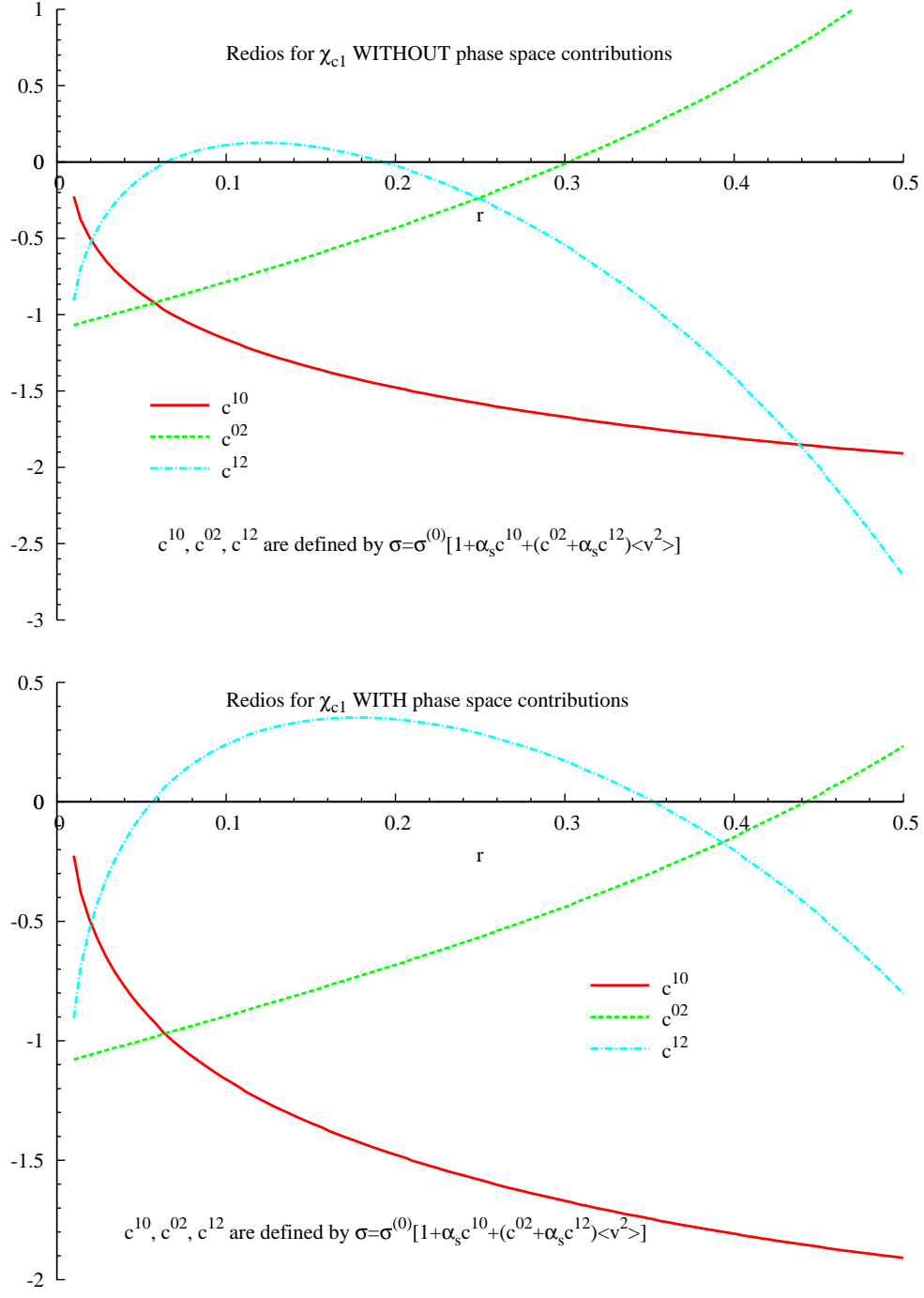


Figure 4. The relative ratios for the corrections in the order of α_s , v^2 , and $\alpha_s v^2$ to the LO cross section for χ_{c1} production recoiled with a hard photon as a function of r . The ratios c^{10} , c^{02} , and c^{11} are defined by the expression $\sigma = \hat{\sigma}^{(0)} [1 + \alpha_s c^{10} + (c^{02} + \alpha_s c^{12}) \langle v^2 \rangle] \langle 0 | \mathcal{O}^H | 0 \rangle$.

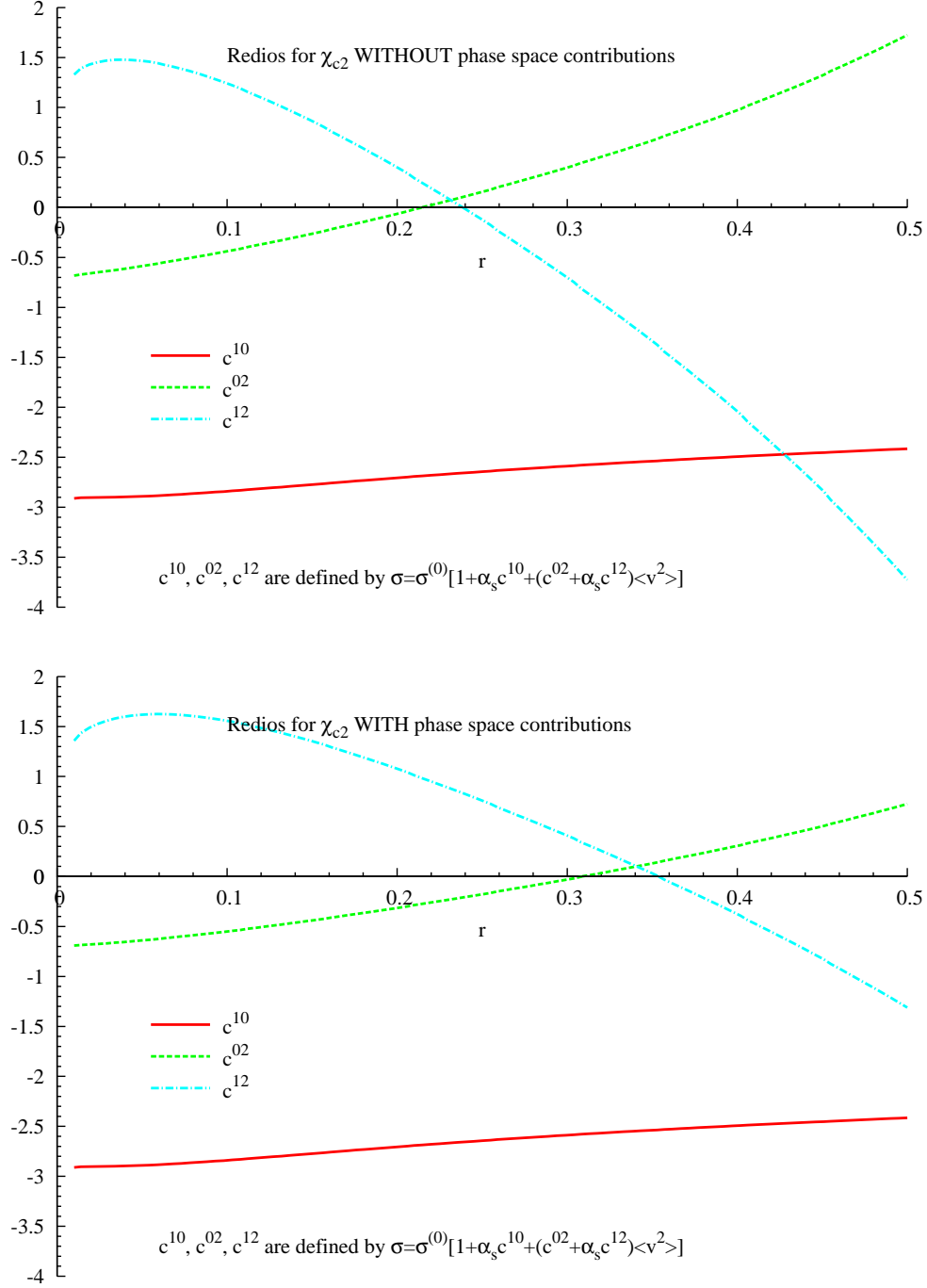


Figure 5. The relative ratios for the corrections in the order of α_s , v^2 , and $\alpha_s v^2$ to the LO cross section for χ_{c2} production recoiled with a hard photon as a function of r . The ratios c^{10} , c^{02} , and c^{11} are defined by the expression $\sigma = \hat{\sigma}^{(0)} [1 + \alpha_s c^{10} + (c^{02} + \alpha_s c^{12}) \langle v^2 \rangle] \langle 0 | \mathcal{O}^H | 0 \rangle$.

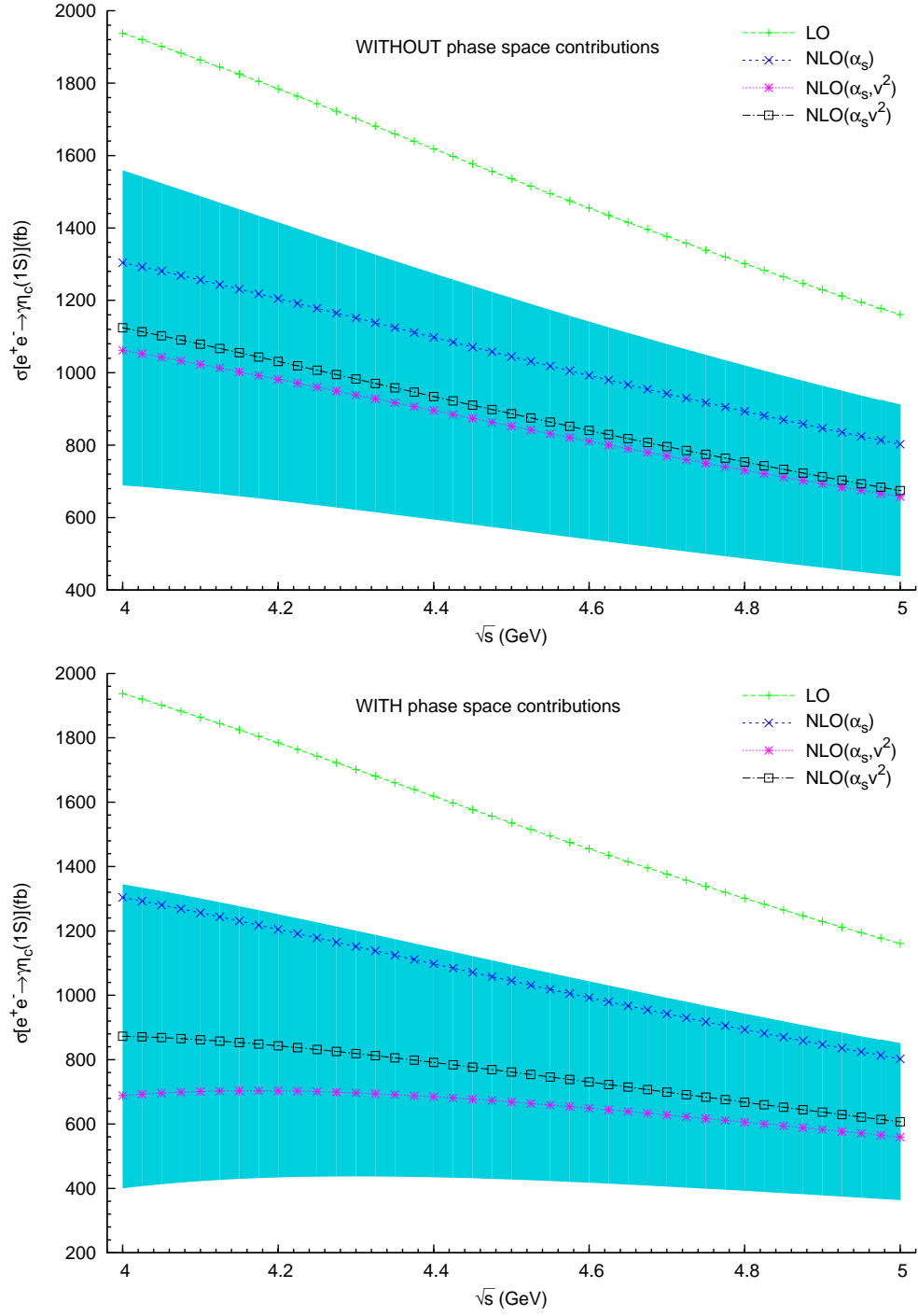


Figure 6. The cross sections of the $\eta_c(1S)$ process at the BESIII energy region. The uncertainties for the total cross sections come from the uncertainties of m_c , α_s , $\langle v^2 \rangle$, and the wave functions at the origin.

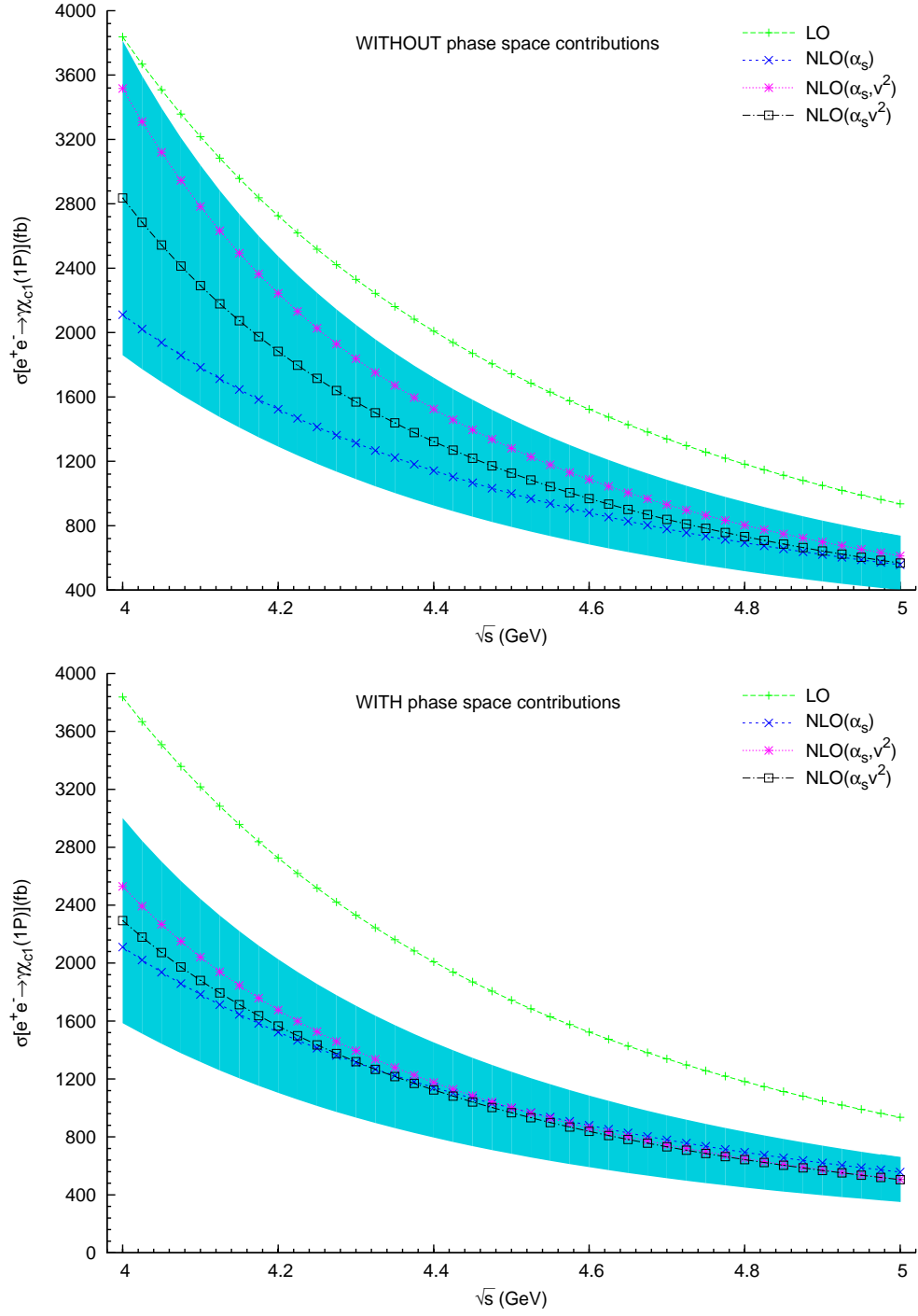


Figure 7. The cross sections of the $\chi_{c1}(1P)$ process at the BESIII energy region. The uncertainties for the total cross sections come from the uncertainties of m_c , α_s , $\langle v^2 \rangle$, and the wave functions at the origin.

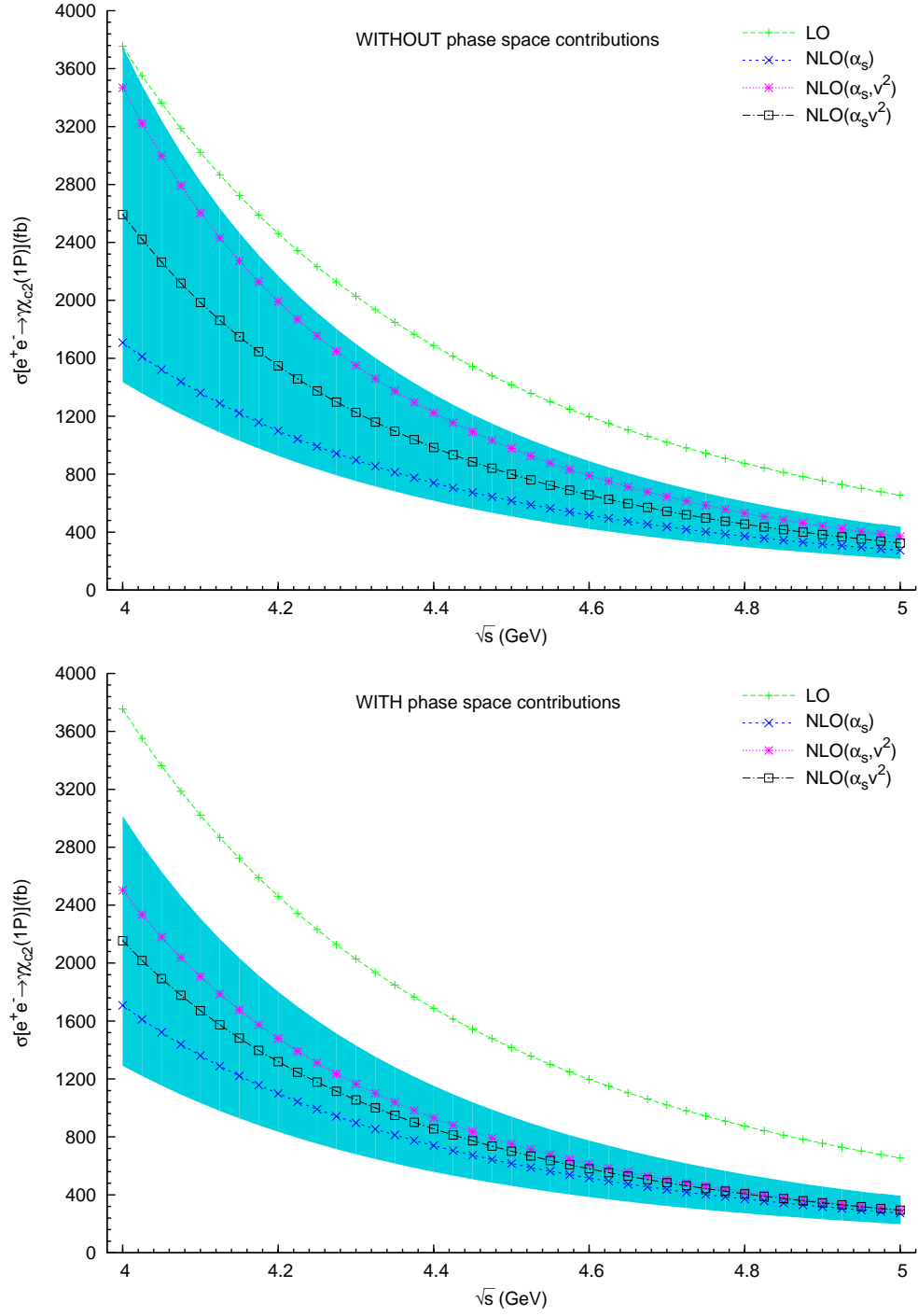


Figure 8. The cross sections of the $\chi_{c2}(1P)$ process at the BESIII energy region. The uncertainties for the total cross sections come from the uncertainties of m_c , α_s , $\langle v^2 \rangle$, and the wave functions at the origin.

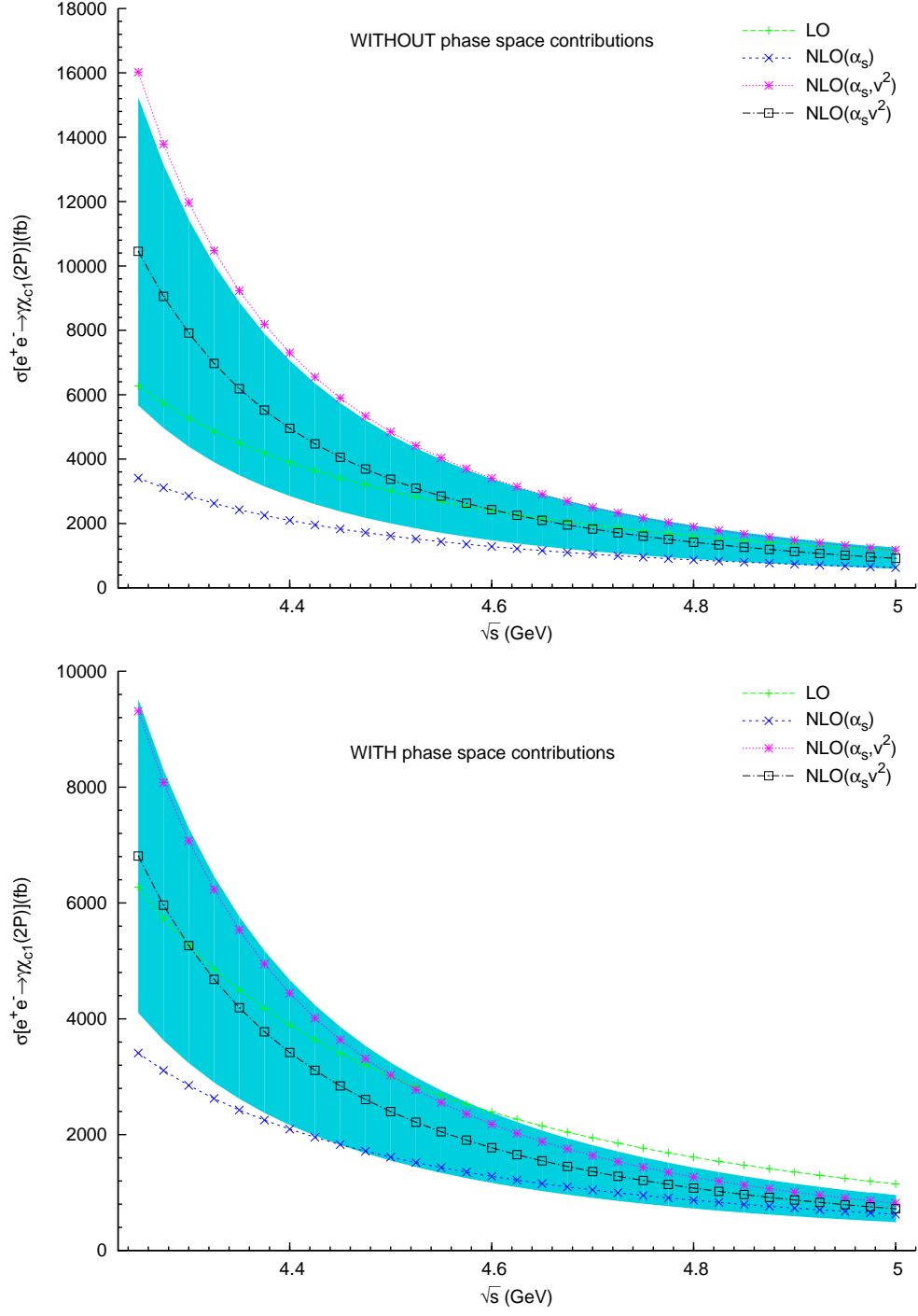


Figure 9. The cross sections of the $\chi_{c1}(2P)$ process at the BESIII energy region. The uncertainties for the total cross sections come from the uncertainties of α_s , $\langle v^2 \rangle$ and the wave functions at the origin.

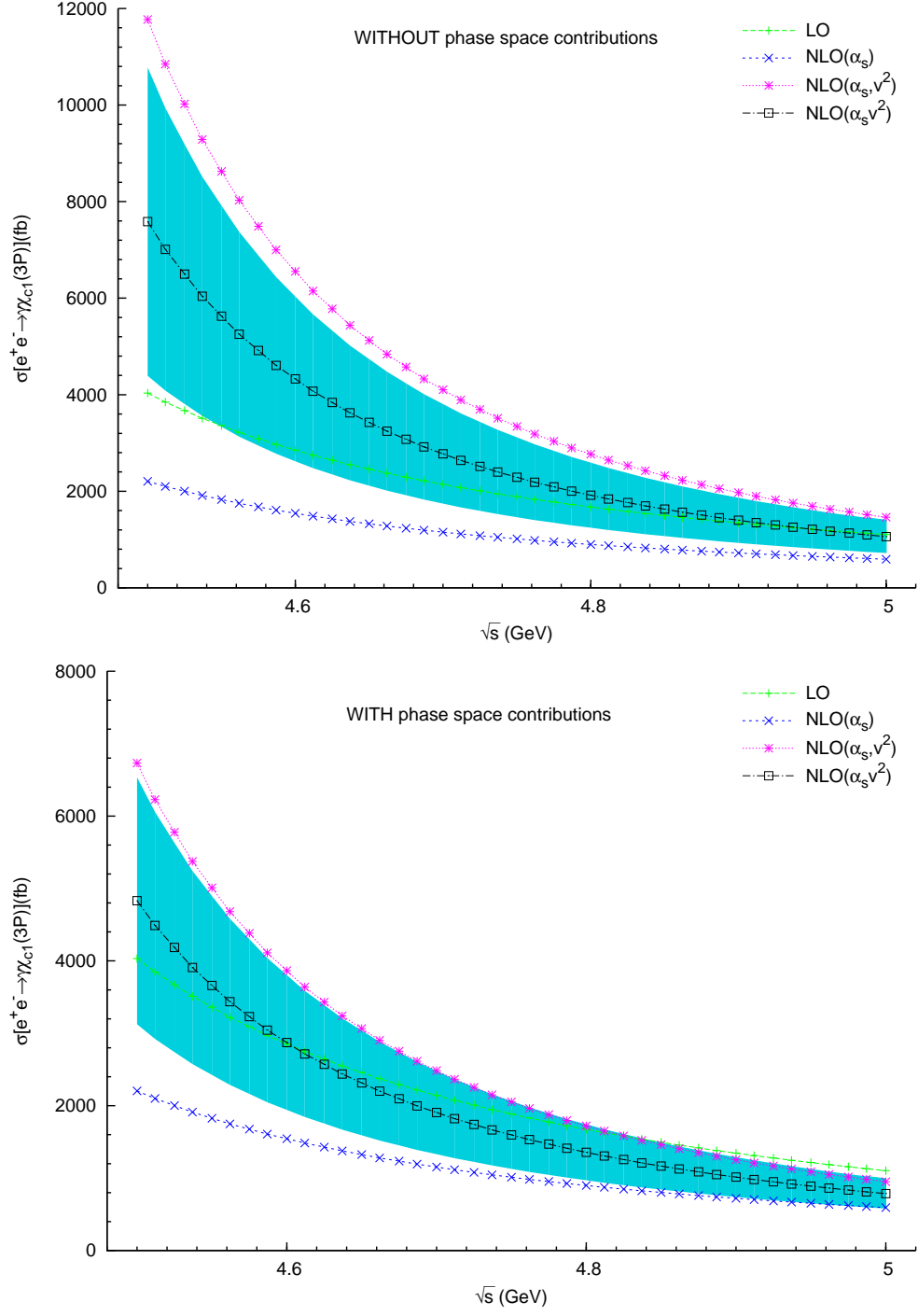


Figure 10. The cross sections of the $\chi_{c1}(3P)$ process at the BESIII energy region. The uncertainties for the total cross sections come from the uncertainties of α_s , $\langle v^2 \rangle$ and the wave functions at the origin.

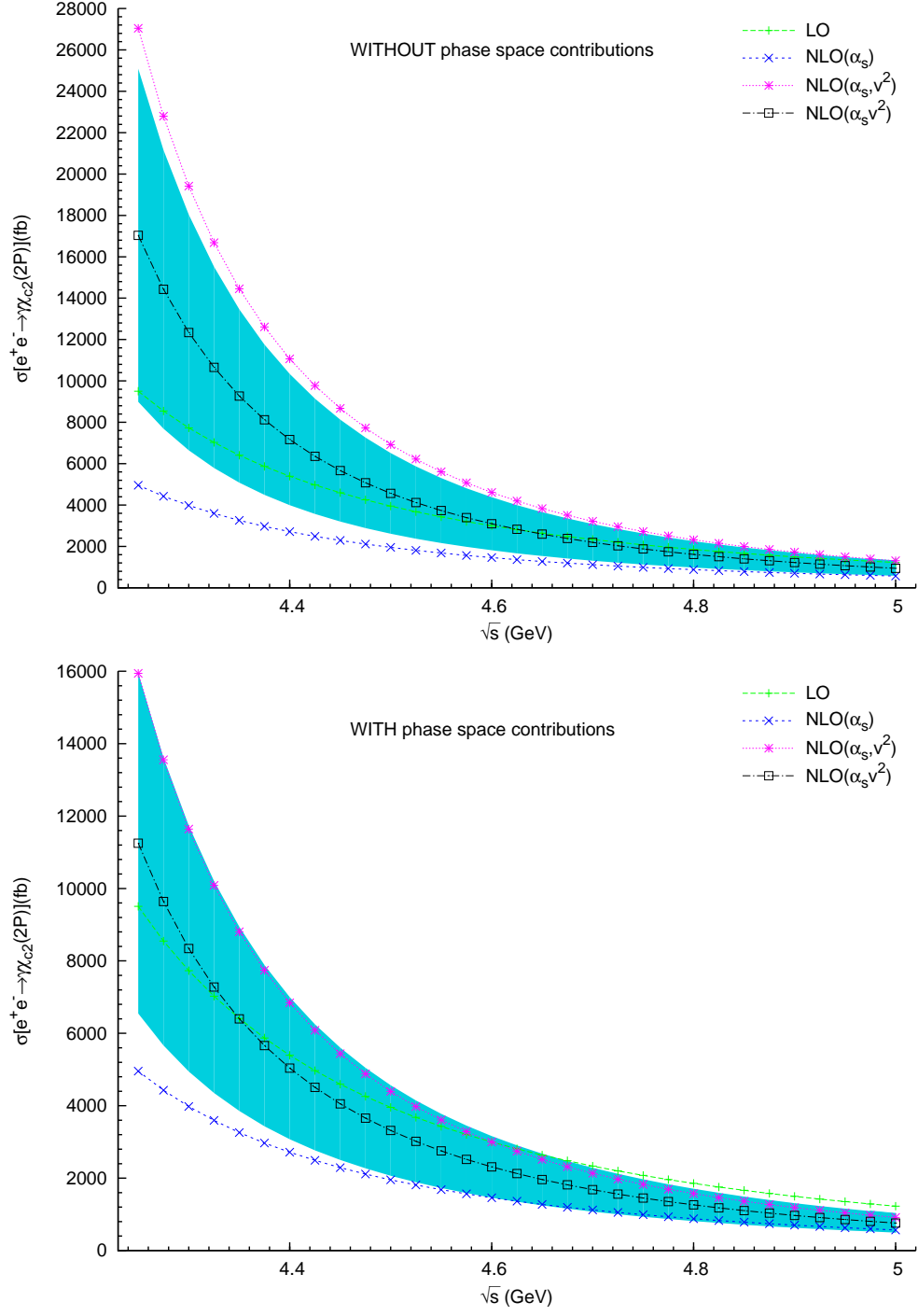


Figure 11. The cross sections of the $\chi_{c2}(2P)$ process at the BESIII energy region. The uncertainties for the total cross sections come from the uncertainties of α_s , $\langle v^2 \rangle$ and the wave functions at the origin.

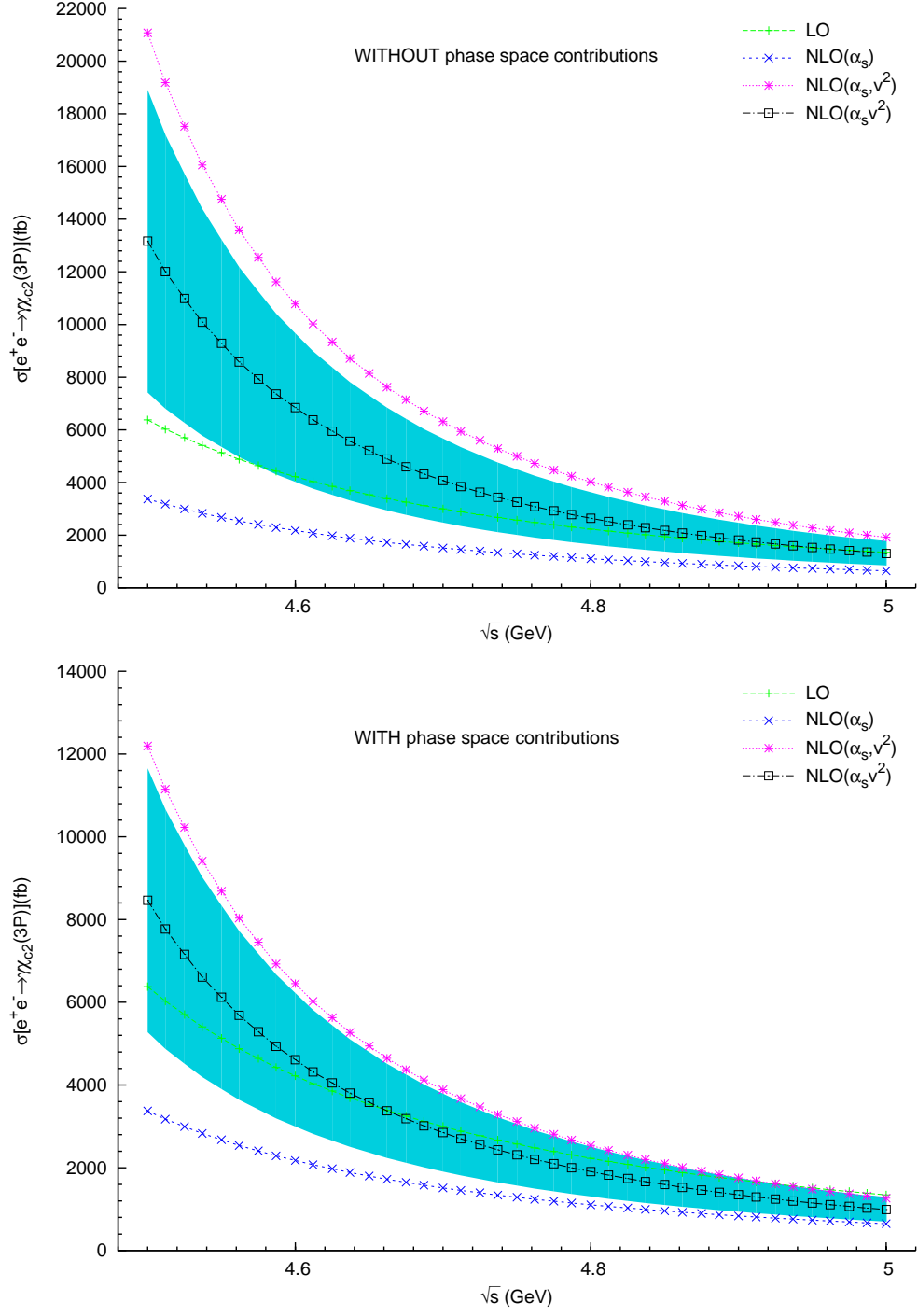


Figure 12. The cross sections of the $\chi_{c2}(3P)$ process at the BESIII energy region. The uncertainties for the total cross sections come from the uncertainties of α_s , $\langle v^2 \rangle$ and the wave functions at the origin.

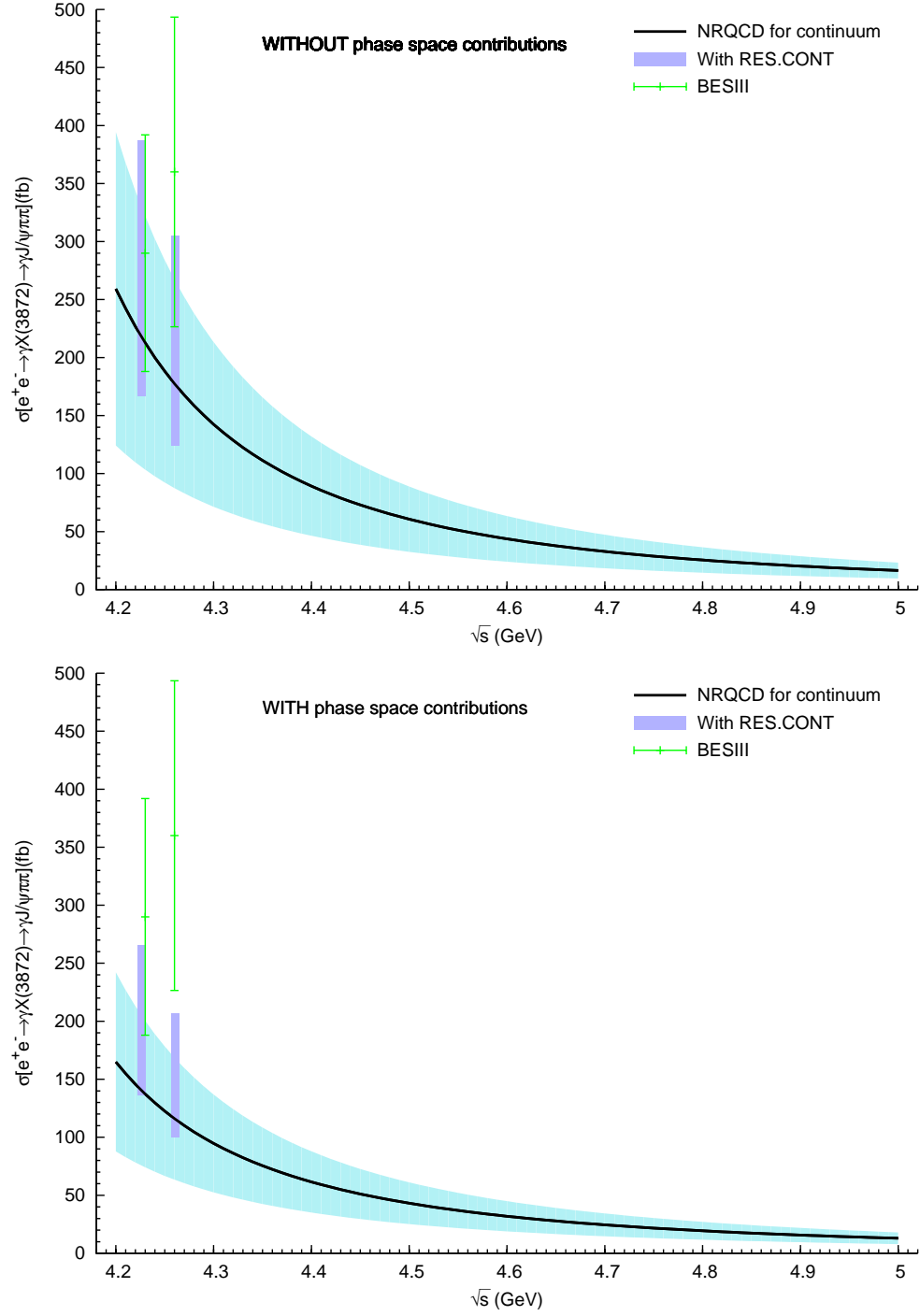


Figure 13. The cross sections of the $X(3872)$ process at the BESIII energy region when taking $X(3872)$ as the mixture with $\chi_{c1}(2P)$ component. The uncertainties for the total cross sections come from the uncertainties of m_c , α_s , $\langle v^2 \rangle$, and the wave functions at the origin. "With RES.CONT" means considering the contributions from both continuum and resonance.